From INSTITUTIONEN FÖR NEUROVETENSKAP
Karolinska Institutet, Stockholm, Sweden

NON-LINEAR SYNAPTIC INTEGRATION ON DENDRITES OF STRIATAL MEDIUM-SPINY NEURON -- A COMPUTATIONAL STUDY

Kai Du

Stockholm 2016

Published by Karolinska Institutet.
Printed by E-Print AB 2016

ISBN 978-91-7676-527-2

Institutionen för Neurovetenskap

Non-linear synaptic integration on dendrites of striatal medium-spiny neuron -- a computational study

AKADEMISK AVHANDLING

som för avläggande av medicine doktorsexnmen vid Karolinska Institutet offtentligen försvaras i Samuelssonsalen, Tomtebodavägen 6.

Måndag den 19 December 2016, kl 13:00-16:00

av

Kai Du

Principal Supervisor:
Professor Jeanette Hellgren Kotaleski
Karolinska Institutet
Department of Neuroscience

Co-supervisor(s):
Professor Sten Grillner
Karolinska Institutet
Department of Neuroscience

Docent Gilad Silberberg
Karolinska Institutet
Department of Neuroscience

Opponent:
Professor Michael Hausser
University College London
Wolfson Institute for Biomedical Research
Division of Medicine

Examination Board:
Professor Patrik Krieger
Ruhr-Universität Bochum
Department of System Neuroscience
Division of Medicine

Professor Gilberto Fisone
Karolinska Institutet
Department of Neuroscience

Docent Pawel Herman
KTH Royal Institute of Technology
Department of Computational Science and Technology
School of Computer Science and Communication

To my wife, *Qin Xiao*.

给我的妻子，肖琴

ABSTRACT

Striatum is the main input nucleus of basal ganglia. Medium-spiny neurons (MSNs), the principal neurons of the striatum, receive convergent excitatory inputs from cortex and thalamus, thus "gate" the information flow to the basal ganglia. The activity of MSNs is further modulated by massive inhibition from their neighboring MSNs as well as from GABAergic interneurons. At corticostriatal synapses in MSNs, a potent and reliable spike timing-dependent plasticity (STDP) can be found. It has been suggested this plasticity follows an "anti-Hebbian" learning rule: pre-synaptic signals preceding post-synaptic action potentials ('pre-post' paring) induces LTD while post-synaptic action potentials preceding pre-synaptic signals ('post-pre' paring) leads to LTP. The long-term potentiation (LTP) relies on NMDAR-mediated calcium influx, while the long-term depression relies on L-type calcium channels and endocannabinoid (eCB) dependent signaling pathways. The sign of STDP rule at the corticostriatal synapses appears to be influenced by the presence of GABAergic inputs. In addition to the role of synaptic interactions for modulating and controlling plasticity, synaptic interactions can also give rise to "dendritic plateaus" were found in MSNs. Clustered activation of spines at distal dendrites, within a short temporal window, can evoke a long-lasting plateau potential in MSNs. It is generally assumed that this supra-linear integration could promote spiking in MSNs, however, it has not been clear how dendritic plateaus are controlled by excitatory and inhibitory inputs in MSNs.

In this thesis, using biophysically detailed models of MSNs, we explored: (1) the possible mechanisms of GABA in STDP formation, (2) the roles of different NMDAR subunits in STDP formation, and (3) how dendritic plateaus affect the integration of excitatory and inhibitory inputs in MSNs. We found that in brain slices the GABA tightly controlled the polarity of STDP in MSNs, while blocking GABA could reverse the STDP rule from anti-Hebbian learning to Hebbian. Surprisingly, the model predicted that GABA depolarizes the dendrites during the STDP protocols and such depolarizing effects further change the balance between NMDA-mediated calcium and the calcium influx from L-type calcium channels. In "pre-post" parings, the GABA strength pushes the balance towards L-type calcium,

thus promoting LTD formation. In contrast, during “post-pre” parings, the presence of GABA pushes the balance more towards NMDAR-mediated calcium, thus favoring LTP formation. Next, we identified the role of NMDAR subunits in LTP formation. The model predicted that the GluN2B subunit could broaden the timing window of LTP. We confirmed the prediction with experiments. At last, we investigated the functional importance of dendritic plateaus in MSNs. The model predicted that dendritic plateaus could enhance neuron-wide integration of excitatory inputs and promote spiking. In contrast, the impact of dendritic inhibition depends on a particular “spatiotemporal” window: the efficacy of dendritic inhibition could be dramatically increased if it is positioned close to the plateau initiation zone and activated within a specific timing window. Intriguingly, the model predicted that such branch-specific inhibition is not due to shutting of $GABA_A$Rs, but relies on the Magnesium (Mg^{2+}) block of NMDARs. We verified the mechanism with two-photon uncaging of glutamate and single-photon uncaging of GABA.

To conclude, we found GABA tightly controlled the direction of STDP in MSNs through depolarizing effects and could effectively suppress the dendritic plateau in MSNs through an NMDAR Mg^{2+} block dependent mechanism.

LIST OF SCIENTIFIC PAPERS

I. Paille, V., Fino, E., **Du, K**., Morera-Herreras, T., Perez, S., Kotaleski, J. H., & Venance, L. (2013). GABAergic circuits control spike-timing-dependent plasticity. *The Journal of Neuroscience*, 33(22), 9353-9363.

II. Evans, R. C., Morera-Herreras, T., Cui, Y., **Du, K.**, Sheehan, T., Kotaleski, J. H., Venance, L. & Blackwell, K. T. (2012). The effects of NMDA subunit composition on calcium influx and spike timing-dependent plasticity in striatal medium spiny neurons. *PLoS Comput Biol*, 8(4), e1002493.

III. **Kai Du**, Yu-Wei Wu , Robert Lindroos, Balázs Rózsa, Gergely Katona, Jun B. Ding, and Jeanette Hellgren Kotaleski. (2016) Dendritic plateau potential enables neuron-wide integration of excitation and branch-specific inhibition in striatal spiny projection neurons. *Manuscript*

CONTENTS

LIST OF ABBREVIATIONS

2PLU	Two-photon laser uncaging
AP	Action potential
ACh	Acetylcholine
AMPA	α -amino-3-hydroxy-5-methyl-4-isoxazolepropionic acid
BK	Large-conductance calcium-dependent potassium channels
bAP	Back-propagating action potential
D1-MSN	Medium spiny neuron mainly expressing D1-receptors
D2-MSN	Medium spiny neuron mainly expressing D2-receptors
EPSC/EPSP	Excitatory postsynaptic current/potential
eCB	Endocannabinoid
E/I	Ratio between excitation and inhibition
FSI	Fast-spiking interneurons
fGABA	Dendritic inhibition with fast kinetics
GABA	Gamma-aminobutyric acid
$GABA_AR$	Gamma-aminobutyric acid type A receptor
HFS	High-frequency stimulation
HH	Hodgkin-Huxley
I-V	Current – voltage
IPSC/IPSP	Inhibitory postsynaptic current/potential
KAf	Fast A-type potassium channels
KAs	Slow A-type potassium channels
KIR	Inward-rectifier potassium channels
KDR	Delayed-rectified potassium channels
LTP	Long-term potentiation
LTD	Long-term depression

LFS	Low-frequency stimulation
mGluR	Metabotropic glutamate receptors
MNI-Glu	4-Methoxy-7-nitroindolinyl-caged-L-glutamate
MSN	Medium-spiny neuron
NMDA	N-methyl-D-aspartate
NMDAR	N-methyl-D-aspartate receptor
NPY-NGF	Neuropeptide Y – neuroglia form
Naf	Fast sodium channels
NaP	Persistent sodium channels
PLTS	Persistent and low-threshold spike
PTX	Picrotoxin
Rubi-GABA	Bis(2,2'-bipyridine-N,N')triphenylphosphine)-4-aminobutyric acid ruthenium hexafluorophosphate complex
STDP	Spike timing-dependent plasticity
SPN	Spiny projection neuron, also called medium-spiny neuron
SK	Small-conductance calcium-dependent potassium channels
sGABA	Dendritic inhibition with slow kinetics
tLTP	Timing dependent long-term potentiation
tLTD	Timing dependent long-term depression
TTX	Tetrodotoxin
uIPSC	Unitary inhibitory postsynaptic current
VSCC	Voltage-sensitive calcium channel

1 BACKGROUND: FROM PHYSIOLOGY TO THEORY

1.1 STRIATUM – INPUT STAGE OF BASAL GANGLIA

The basal ganglia are subcortical nuclei which are critical for action initiation and selection (Tepper, Koos et al. 2004, Gittis and Kreitzer 2012). The basal ganglia circuitry mainly consists of the striatum, globus pallidus external and internal, subthalamic nucleus and substantia nigra. As the main entrance to basal ganglia, the striatum receives massive glutamatergic inputs mainly from cortex and thalamus (Smith and Bolam 1990, Gerfen 1992, Smith, Raju et al. 2004) . The excitatory afferents to the striatum carry abundant information containing sensory, motor, cognitive and limbic signals (Gittis and Kreitzer 2012). In addition to glutamatergic inputs, the striatum is also innervated by dense dopaminergic inputs from midbrain (Surmeier, Plotkin et al. 2009, Gerfen and Surmeier 2011). Dopamine is a critical modulator to striatal function, while loss of dopamine neurons will cause motor disorders, such as Parkinson's disease (Surmeier, Plotkin et al. 2009, Gerfen and Surmeier 2011).

A unique feature of the striatal circuitry, in particular compared to other main regions in our brain, is the complete lack of glutamatergic neurons (Tepper, Koos et al. 2004, Gittis and Kreitzer 2012). The vast majority of neurons in the striatum are GABAergic medium spiny neurons (MSNs), also called spiny projection neurons (SPNs) (Tepper, Koos et al. 2004, Gittis and Kreitzer 2012). MSNs account for approximately 90% of the total striatal populations and give rise to collateral inhibition to their surrounding MSNs, usually via synapses on the middle to distal dendrites of neighboring MSNs (Tepper, Koos et al. 2004, Gittis and Kreitzer 2012).

The prevailing working theory of striatum (and also for the basal ganglia) is the balance between the direct ('go') and the indirect ('no-go') pathway (Gerfen and Surmeier 2011). Two main subpopulations of MSNs in the striatum give rise to two pathways via their projection destinations and gene expression patterns (Tepper, Koos et al. 2004, Gittis and Kreitzer 2012): one group of MSNs project directly to the output nuclei of basal ganglia ('direct-pathway') and mainly express D1-receptors (D1-MSNs), while another population of MSNs project to intermediate part of basal ganglia (globus pallidus external) and mainly express D2-receptors (D2-MSNs). The direct-pathway facilitates action selections while the indirect-pathway opposes actions. Thus, the output of striatum (and even of the whole basal ganglia) could heavily reply on competition between these two pathways—the winning pathway would suppress its opponent (Tepper, Koos et al. 2004). However, this 'winners-take-all' model has been be challenged by *in vivo* calcium imaging data, which showed co-activation of direct and indirect pathways in the striatum when initiating certain actions (Cui, Jun et al. 2013).

I will introduce more details regarding MSNs and the main interneurons below.

1.1.1 Striatal neurons

Because MSNs are dominant with regards to numbers in the striatum, most of the cortical and thalamic inputs are converged onto MSN dendrites (Smith and Bolam 1990, Gerfen 1992, Smith, Raju et al. 2004). Thus, MSNs "gate" the information flow from cortex/thalamus to the basal ganglia output stages and likely are the most important neurons of basal ganglia.

The morphological and electrophysiological features of MSNs are different from cortical and hippocampal pyramidal neurons which are perhaps most well studied neurons in the brain. Pyramidal neurons have long apical dendrites but relatively short basal dendrites. In contrast, dendrites of MSNs are much shorter (~200 um), and the dendritic tree looks more like spherical "ball" in its natural form (Tepper, Koos et al. 2004, Wilson 2007, Gittis and Kreitzer 2012). Unlike pyramidal neurons that have long primary dendrites over 100 um, MSNs are endowed with short primary dendrites (~10-30 um) , rapidly evolving into very thin dendrites (Gertler, Chan et al. 2008) ; such dendritic structure might make MSNs electronically more "compact" than cortical pyramidal neurons (Gertler, Chan et al. 2008) .

Due to high density of inward-rectifier potassium channels (Kir) and A-type potassium channels (KA), MSNs normally display hyperpolarized resting membrane, near the K+ equilibrium potentials at around -80 to -90 mV, often called "down-state" (Wilson and Kawaguchi 1996, Stern, Kincaid et al. 1997) . *In vivo* (but under anesthesia), MSNs were observed to transit from the hyperpolarized "down-state" to a depolarized "up-state" (-60 to -55 mV); it appears action potentials can only be triggered during the up-state (Wilson and Kawaguchi 1996, Stern, Kincaid et al. 1997, Stern, Jaeger et al. 1998). In order to achieve this ~20 to 30 mV "jump" between the "down-state" and "up-state", it has been estimated that a large number (hundreds to thousands) of coherent inputs would be required to drive MSNs (Wilson and Kawaguchi 1996, Stern, Kincaid et al. 1997, Stern, Jaeger et al. 1998, Wolf, Moyer et al. 2005). It was recently found that activating a small number of spines in distal dendrites within a short timing window could induce long-lasting plateaus in the soma, mimicking the up-state of MSNs (Plotkin, Day et al. 2011). Such dendritic plateaus require much less (tens) excitatory inputs and could efficient promote MSN membrane potential state-transition (Plotkin, Day et al. 2011).

The striatal interneurons are mostly GABAergic as well, which can be divided into two classes (Kawaguchi 1993, Gittis and Kreitzer 2012):

- fast-spiking interneurons (FSI) expressing parvalbumin (PV)
- persistent and low-threshold spike (PLTS) interneurons but expressing somatostatin (SOM), neuropeptide Y (NPY), and nitric oxide synthase (NOS) respectively.

In addition to GABAerigic interneurons, there are a small number of Cholinergic interneurons in the striatum, which release the neurotransmitter acetylcholine (ACh) and modulate the local GABAerigic circuitry (Witten, Lin et al. 2010, English, Ibanez-Sandoval et al. 2011, Oldenburg and Ding 2011).

1.1.2 Intrastriatal synaptic interactions

There are couple of rules that how these GABAergic neurons target:

- FSIs mostly target on the perisomatic regions of MSNs (Kubota and Kawaguchi 2000, Straub, Saulnier et al. 2016).
- PLTSs mostly target on the distal dendrites of MSNs (Kubota and Kawaguchi 2000, Straub, Saulnier et al. 2016).

The most well studied interneurons are FSIs, which usually induce large amplitude and fast kinetic unitary IPSCs (uIPSC) on MSNs (Gittis, Nelson et al. 2010, Planert, Szydlowski et al. 2010). *In vitro* experiments have shown that FSIs normally have much lower firing threshold than MSNs. The same somatic current injection only induced subthreshold depolarization in MSNs, but would evoke spike trains in FSIs (Gittis, Nelson et al. 2010, Planert, Szydlowski et al. 2010). Therefore, cortical inputs could easily trigger a train of action potentials in FSIs. Since FSIs activate a train of IPSCs on MSNs and their terminals directly target on perisomatic areas near action potential initiation zone, it is generally believed that FSIs can strongly inhibit firing of MSNs and thus powerfully inhibit the striatal network (Tepper, Koos et al. 2004). However, it is worthy to note that IPSC trains from FSIs to MSNs display short-term plasticity with strong depression (Planert, Szydlowski et al. 2010), suggesting that the influence of FSIs might not be as powerful as we previously expected.

Compared to FSIs, PLTS interneurons mainly project to distal MSN dendrites and evoke relatively small amplitude and fast kinetic uIPSCs (Gittis, Nelson et al. 2010, Straub, Saulnier et al. 2016) . It is not clear how PLTS interneurons modulate MSNs through GABA release. PLTS interneurons might modulate the output of MSNs with neuromodulations, such as somatostatin (SOM), neuropeptide Y (NPY) and nitric oxide (NO) (Gittis and Kreitzer 2012).

It was recently found that a small group of interneurons, neuropeptide Y-neurogliaform (NPY-NGF) interneurons induce slow kinetic uIPSCs on MSNs (Ibanez-Sandoval, Tecuapetla et al. 2011). The NPY-NGF interneurons also target distal dendrite of MSNs (Ibanez-Sandoval, Tecuapetla et al. 2011). Interestingly, NPY-NGF interneurons have surprisingly high connectivity to local MSNs (~67-80%) (Ibanez-Sandoval, Tecuapetla et al. 2011), suggesting they might play important roles in regulating the striatal network.

1.1.3 Synaptic plasticity and learning in the striatum

Synaptic strength can be modulated by pre- and/or post-synaptic activities. Early in 1949, Hebb proposed that “when an axon of cell A is near enough to excite a cell B and repeatedly or persistently takes part in firing it, some growth process or metabolic change takes place in one or both cells such that A’s efficiency, as one of the cells firing B, is increased” (Hebb 1949) – a pioneering theory that defined ‘use-dependent’ changes in synaptic efficacy , also termed as *Hebb’s rule*. In line with the Hebb’s rule, experiment evidence of long-term potentiation (LTP) was first discovered by applying high-frequency stimulation (HFS) to the pre-synaptic afferents in hippocampus (Bliss and Gardner-Medwin 1973, Bliss and Lomo

1973). In contrast, long-term depression (LTD) was discovered in cerebellum by low-frequency stimulation (LFS) of parallel fibers and climbing fibers (Ito and Kano 1982). Today, LTP and LTD are found at many glutamatergic synapses in nearly every brain regions and are considered as fundamental rules for learning and memory (Siegelbaum and Kandel 1991, Bliss and Collingridge 1993, Caporale and Dan 2008).

Traditionally, LTP is induced by HFS while LTD is induced by LFS (with or without post-synaptic depolarization) (Siegelbaum and Kandel 1991, Bliss and Collingridge 1993, Caporale and Dan 2008). Is the temporal order of stimulation important for LTP or LTD induction? A novel plasticity paradigm correlated to temporal sequences of induction protocols was discovered in the 90's and was termed as "spike timing-dependent plasticity (STDP)" (Magee and Johnston 1997, Markram, Lubke et al. 1997, Bi and Poo 1998, Debanne, Gähwiler et al. 1998) . STDP is the synaptic strength determined by the relative timing between pre-synaptic inputs (such as EPSPs) and post-synaptic action potentials (APs) (Magee and Johnston 1997, Markram, Lubke et al. 1997, Bi and Poo 1998, Debanne, Gähwiler et al. 1998, Caporale and Dan 2008). For example, in neocortex if the excitatory afferent signals proceed APs ('pre-post'), timing-dependent long-term potentiation (tLTP) will be induced at pyramidal neuron synapses; the reverse order between pre- and post-synaptic signals ('post-pre') would induce timing-dependent long-term depression (tLTD) (Caporale and Dan 2008). Subsequent works further reveal that STDP widely exist at glutamatergic and even GABAergic synapses in our brain (Caporale and Dan 2008). It is noteworthy that because STDP induction is critically dependent on the amplitude of back-propagating action-potentials (bAPs), the location of synapses in dendrites are important (Froemke, Poo et al. 2005, Sjostrom and Hausser 2006, Froemke, Letzkus et al. 2010). For instance, dendritic locations of synapses could shape the timing-window (Froemke, Poo et al. 2005) and even reverse the direction of plasticity when moving from the soma to distal dendrite (Sjostrom and Hausser 2006). Because STDP records timing of synaptic events, it links the "causality" in the activation protocols to the direction of STDP (potentiation or depression). Thus, the STDP rule expands the original "Hebb's rule" to a wide variety of learning rules in our brain (Caporale and Dan 2008, Froemke, Letzkus et al. 2010), although the role of STDP *in vivo* is still in debate (Markram, Gerstner et al. 2012). Nowadays, the term "Hebbian-learning" appears to be more related to STDP rules.

The cellular mechanisms underlying STDP might vary at different brain regions. In neocortical (Froemke, Poo et al. 2005, Nevian and Sakmann 2006) and hippocampal neurons (Magee and Johnston 1997), it appears that tLTP relies on boosting of calcium influx though NMDARs. In contrast, tLTD is dependent on inactivation of NMDARs via calcium influx from voltage-sensitive calcium channels (VSCC). In other brain regions such as in barrel cortex , tLTD is not dependent on NMDARs , but relies on activation of postsynaptic metabotropic glutamate receptors (mGluR) and VSCC (Sjostrom, Turrigiano et al. 2003, Nevian and Sakmann 2006), which further promote the synthesis and release of endocannabinoid (eCB) (Hashimotodani, Ohno-Shosaku et al. 2005, Hashimotodani, Ohno-Shosaku et al. 2007).

In the striatum, the most well studied plasticity is LTD induced by paring postsynaptic depolarization with high frequency afferent inputs (Lovinger, Tyler et al. 1993, Kreitzer and Malenka 2005). The induction of such LTD requires postsynaptic release of eCB (Gerdeman, Ronesi et al. 2002). It was suggested that the eCB-dependent LTD largely relies on boosts of L-type calcium (Adermark and Lovinger 2007). Recently, STDP was also found in MSNs (Fino, Glowinski et al. 2005, Shen, Flajolet et al. 2008). However, the findings of STDP appear to be controversial. In slice preparations when GABAergic circuitry was kept as intact as possible, the STDP at corticostriatal synapses follows an "anti-Hebbian" rule (Fino, Glowinski et al. 2005): the "pre-post" paring leads to tLTD, while the reverse order of pre- and post-synaptic signals induces tLTP. In contrast, when $GABA_A$Rs were pharmaceutically inhibited, "Hebbian" rule was observed in MSNs (Shen, Flajolet et al. 2008). Further experiments were required to explore the roles of GABA in STDP inductions in MSNs. Similar to tLTP in cortex, tLTP at corticostriatal synapses is dependent on NMDAR activation (Shen, Flajolet et al. 2008, Surmeier, Plotkin et al. 2009, Gerfen and Surmeier 2011). On the other hand, tLTD at corticostriatal synapses relies on eCB signaling via L-type VSCC activation, in particular, the Ca_V 1.3, a low-voltage activated calcium channels. Also the corticostriatal plasticity is dependent on neuromodulation via e.g. dopamine (Shen, Flajolet et al. 2008, Surmeier, Plotkin et al. 2009, Gerfen and Surmeier 2011).

1.2 NON-LINEAR DENDRITIC COMPUTATION

1.2.1 Introduction to dendritic computation

Traditionally, many spiking neuron models treat a single neuron as a "point-device" when aiming to model the spiking behavior of real neurons (Brunel et al., 2014). Examples are leaky integrate-and-fire (LIF) model, the generalized two-variable integrate and-fire (GIF) model and the exponential integrate-and-fire (EIF) model (Brunel et al., 2014). These simplified "point" neuron models can nicely fit complex firing patterns from diverse types of neurons. However, both theoretical and experimental progress in the last decade have proposed that a single neuron can process inputs as a multi-layer computational device, in which individual dendritic branches act as a functional unit (Poirazi, Brannon et al. 2003, Branco and Hausser 2010, Major, Larkum et al. 2013, Stuart and Spruston 2015) . In many brain regions, neuronal dendrites are capable of performing comprehensive computations on excitatory synaptic inputs (London and Hausser 2005, Losonczy and Magee 2006, Silver 2010, Major, Larkum et al. 2013, Brunel, Hakim et al. 2014). One perhaps the most comprehensive hypothesis for computing mode of cortical pyramidal neurons is the "3-layer network" proposed by (Hausser and Mel 2003), suggesting that computations are likely performed in three stages: at distal dendrite, at proximal dendrite and at the soma, respectively. This theory was later elaborated on by direct dendritic recordings far distal from the soma (Larkum, Nevian et al. 2009), and the experiments revealed "chained reactions" between NMDARs and ion channels: NMDA spikes evoked at distal dendrite first triggers 'calcium-spikes' by activating local calcium channels, then, during its propagation to

the soma, the NMDA spike is further facilitated by the "sodium spike" in the proximal dendrite. To conclude, the non-linear signal integration in neuronal dendrites rely on at least three factors: (1) non-linear properties of NMDARs, (2) boosting of ion channels, and (3) local input impedance due to morphology patterns.

1.2.2 Dendritic plateaus in the striatum

In this section, I will mainly introduce a particular dendritic nonlinearity, "dendritic plateaus", which were observed in MSNs as well as in many other neurons.

In vitro, "dendritic plateaus" are electronic regenerative events observed in distal dendrites of many types of neurons, including Purkinje-cell (Campbell, Ekerot et al. 1983), spinal interneurons (Kiehn, Johnson et al. 1996), cortical pyramidal neurons (Takahashi and Magee 2009) and striatal MSNs (Plotkin, Day et al. 2011), where spatiotemporally clustered inputs can lead to strong depolarization in the soma, lasting for hundreds of milliseconds. *In vivo* experiments demonstrate that dendritic plateaus can amplify excitatory signals, promote plasticity, thus enhance neuron's capacity of learning and information storage at particular branch (Lavzin, Rapoport et al. 2012, Xu, Harnett et al. 2012, Gambino, Pages et al. 2014).

With respect to MSNs, dendritic plateaus were shown to be an efficient way to drive the cell membrane switching from the "down-state" to the "up-state" (Plotkin, Day et al. 2011). There are several factors which would affect the generation of dendritic plateaus in MSNs (Plotkin, Day et al. 2011): First, it was location-dependent and only clustered activation of spines in distal dendrites would induce plateaus, while activating clustered spines in proximal dendrite only gave rise to transient depolarization. Secondly, plateau potentials are NMDAR-dependent and blocking NMDAR will completely abolish plateaus. Thirdly, it is dependent on T-type and R-type calcium channels, but not L-type calcium channels. Blocking T-type or R-type calcium channels would significantly attenuate the width of plateaus. At last, dopamine differentially modulate plateaus on D1- and D2-MSNs: agonists of D1-receptors would prolong the duration of the plateau, while agonists of D2-receptors would shrink the duration of the plateau.

The dendritic plateau produced in MSNs appear to lack a sodium "spikelet", a hallmark of NMDA spikes/plateaus observed in cortical pyramidal neurons (Schiller, Major et al. 2000). Due to high density of sodium channels in pyramidal neuron dendrites, synaptic excitation will evoke sodium transients in the dendrite – the sodium "spikelet"– preceding the plateau, helping to facilitate initiation of plateaus (Schiller, Major et al. 2000). In contrast, due to low density of sodium channels in distal MSN dendrites (Day, Wokosin et al. 2008), the sodium spikelet appears to be absent in plateau potentials of MSNs (Plotkin, Day et al. 2011). The absence of a sodium spikelet in plateau potentials suggests that the threshold of evoking a plateau might be higher in MSNs than in pyramidal neurons.

1.2.3 Voltage-sensitivity of NMDARs

Dendritic plateaus are generally viewed as an "augmented version" of NMDA spikes (Antic, Zhou et al. 2010). Understanding the intrinsic kinetics of NMDARs is critical for exploring the computation power of plateau potentials.

Activation of NMDARs relies on: (1) binding to glutamate and opening of the synaptic channel, (2) removal of magnesium (Mg^{2+}) ions (Antic, Zhou et al. 2010, Major, Larkum et al. 2013). In the first process, binding to glutamate is assumed to be instantaneous, but opening/closing of the synaptic channel is a slow process and independent of membrane voltage (Eq. 1.2). The second process—removal of Mg^{2+} — is also instantaneous but voltage-dependent (Eq. 1.3). The classic phenomenological model of NMDAR captures these two process (Zador, Koch et al. 1990):

$$g_K NMDA\ (V,t) = g_k(t) f_{Mg-block}(V) \quad (1.1)$$

$$g_k(t) = \frac{A*gmax}{\tau 1-\tau 2}\ (e^{-\frac{t}{\tau 1}} - e^{-\frac{t}{\tau 2}}) \quad (1.2)$$

$$f_{Mg\_block}(V) = \frac{1}{1+\eta[Mg^{2+}]e^{-rV}} \quad (1.3)$$

Here, A is the normalized constant, gmax is maximal conductance, τ1 and τ2 are rising/decaying time constants, respectively.

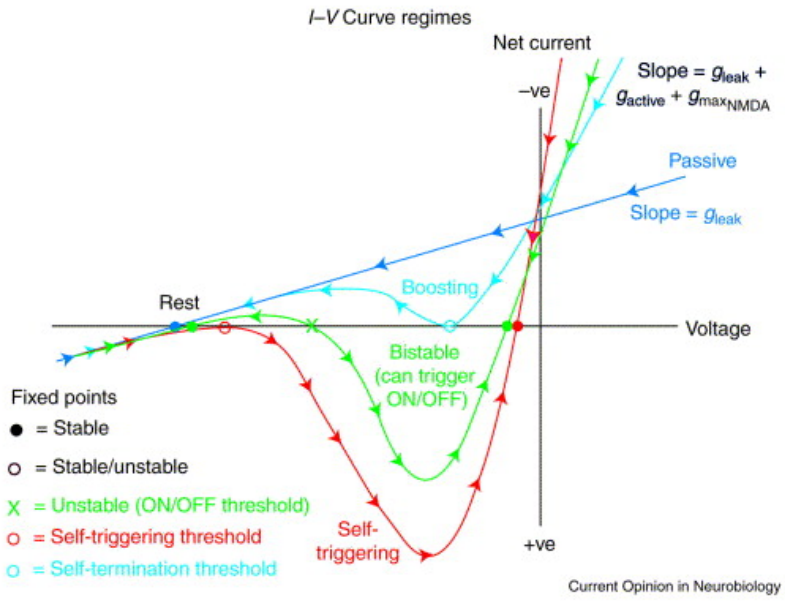

Figure 1. I-V curves of NMDARs. All slopes present sum of leak conductance (g_{leak}), active channels (g_{active}) and maximal NMDA conductance (g_{max}NMDA) included in the system. Arrows indicate directions if the system at particular voltage would move towards or away from the fixed point. Taken from (Schiller and Schiller 2001) with permission.

The non-linear Mg^{2+} blocking effect on NMDARs (Eq. 1.3) endows NMDARs with an intriguing feature of voltage sensitivity. The bell-shaped "current-voltage" (I-V) curves revealed three types of regimes (Fig.1): "Boosting", "Bistable" and "Self-triggering" (Schiller and Schiller 2001). When the maximal conductance of NMDAR ($g_{max}NMDA$) is small, it can always induce "increased" EPSPs/depolarizations and quickly go back to the resting state ("Boosting" state in Fig.1). Increasing the amount of $g_{max}NMDA$ will shift the I-V curves from boosting regions to "Bistable". There is a "threshold" in the Bistable state (the "X" of the green line in Fig.1) which determines if NMDAR can trigger plateau potentials or not. Further adding $g_{max}NMDA$ will push the I-V curve into the "self-triggering" zone, where the NMDARs always induce self-sustained plateau potentials (Schiller and Schiller 2001).

1.2.4 Impact of dendritic inhibition on the plateau potential

Compared to the role of dendritic plateaus, a supra-linear integration of excitatory synaptic inputs, little is known about how dendritic inhibition interacts with plateau potentials. A theoretical work on layer-5 Pyramidal neuron suggested that if GABA conductance was positioned in the same branch where dendritic plateaus were initiated, it would be most efficient to prevent the initiation of plateaus or even to collapse the plateau (Rhodes 2006). Moreover, the timing of GABA should be in a precise time window of 30 ms – right before or after the plateau was induced (Rhodes 2006). It was suggested that the mechanism for this branch-specific inhibition is due to the electronic geometry of distal dendrites (Rhodes 2006). Similar conclusions were made in another study about dendritic inhibition on NMDA spikes in layer-5 Pyramidal neuron (Jadi, Polsky et al. 2012). Combing computational and experimental techniques, it was shown that dendritic inhibition controls the gain and threshold of NMDA spikes depending on its distance relative to NMDA spike initiation region. It appears that the authors of this paper attributed the inhibition effects to "shutting" via GABA channels (Jadi, Polsky et al. 2012).

1.3 MODELING "REALISTIC" NEURONS

Because building biophysically detailed MSN model is the core of this thesis, in this section, I will give a brief introduction to the simulation environment and key points pertinent to construct a "realistic" neuron model from scratch.

1.3.1 Why we need detailed modeling?

Biophysically detailed modeling is a powerful tool to explore dendritic computation of single neuron and can deepen our understanding on the computational complexity of the brain. The detailed modeling aims to capture detailed biophysical features of neurons, including their morphological and electrophysiological properties. Integrating realistic neuron models into large-scale network models is expected to reconstruct complex brain circuitry (Markram, Muller et al. 2015).

The challenge in building a detailed neuron model is parameter tuning, as dozens of parameters in a single neuron model need to be tuned to fit a wide range of experiment data. Lacking data for ion channel distribution, in particular their distribution on dendrites, is one obstacle for constructing detailed models. The first well-known realistic model was the famous Purkinje-cell model made in the middle of the 90's (De Schutter and Bower 1994). A growing number of realistic neuron models have been made and gathered in the public database "ModelDB" hosted by Yale University (Hines, Morse et al. 2004). The pioneering work of constructing large-scale realistic brain circuitry is the European *Human Brain Project* (HBP) (Markram, Muller et al. 2015), which will further boost the wave of detailed neuron modeling in the neuroscience community.

1.3.2 Modeling tools

The GEneral NEural SImulation System (GENESIS) (Bower and Beeman 2007) was the first simulator for detailed neuron models built in 1988 at Caltech, followed by NEURON (Hines and Carnevale 1997) and MOOSE (Ray and Bhalla 2008). Today, these tools are the most popular simulators in computational neuroscience community when building detailed neuron models. These simulators cover a wide range of functions such as building subcellular pathways, multi-compartment neuron model and large-scale networks. A really detailed neuron model contains tens of thousands differential equations, therefore the speed and accuracy for solving massive "coupled" differential equations is critical for running detail models. Hines developed an algorithm to solve such large scale differential equations in this particular type of simulated neural system (Hines 1984). The Hine's solver was implemented in GENESIS and NEURON. Hence, by far these two simulators have been the most efficient and reliable simulators for single detailed neuron or large-scale realistic neuronal network simulations.

GENESIS is the main simulator used in this thesis, which can be installed in Unix/linux/Mac OS environment, but not for Windows system. It has a serial version and parallel version for single work station and parallel computers, respectively. The serial GENESIS is the core simulator, which takes care of all actual computations, while the parallel GENESIS (PGENESIS) works as an "envelope" on top of serial GENESIS. In conjunction with other software such as MPI or PVM, PGENESIS can support large-scale network simulations on supercomputers. Further details of GENESIS simulators can be found in the on-line tutorial "the Book of GENESIS" (James M. Bower and Beeman 2003).

MOOSE (Multiscale Object-Oriented Simulation Environment) is a simulator developed based on GENESIS but "encapsulated" with Python programmatic interface (Ray and Bhalla 2008). MOOSE inherits the GENESIS parser (Ray and Bhalla 2008). With its Python-interface, it would be much easier to interact with other simulators (such as NEURON) or to incorporate other software in scientific community (Ray and Bhalla 2008). NEST (NEural Simulation Tool) is a simulator dedicated to large-scale network of "point" neurons but can also be used for multi-compartment models (Gewaltig and Diesmann 2007). MUSIC is a standard API and can work as an interface allowing different simulators, such as NEURON,

MOOSE and NEST, to exchange data during runtime (Djurfeldt, Hjorth et al. 2010). STEPS (STochastic Engine for Pathway Simulation) is a subcellular simulation environment released by the European Human Brain Project (Hepburn, Chen et al. 2012).

1.3.3 Modeling ion channels

The classic Hodgkin-Huxley (HH) Model is a standard phenomenological model for ion channels (Hodgkin and Huxley 1952, Hodgkin and Huxley 1952). Taking the sodium channel as an example, the conventional HH formula for sodium conductance can be summarized as follows:

$$G_{Na} = g_{Na} m^3 h \quad (1.4)$$

$$\frac{dm}{dt} = \alpha_m(V)\,(1-m) - \beta_m(V)m \quad (1.5)$$

$$\frac{dh}{dt} = \alpha_h(V)\,(1-h) - \beta_h(V)h \quad (1.6)$$

$$m_\infty(V) = \frac{\alpha_m(V)}{\alpha_m(V)+\beta_m(V)} \quad (1.7)$$

$$\tau_m(V) = \frac{1}{\alpha_m(V)+\beta_m(V)} \quad (1.8)$$

$$m(t) = m_\infty - (m_\infty(V) - m_\infty(V_0))e^{-\frac{\tau_m}{t}} \quad (1.9)$$

,where *m* and *h* stands for an *activation* and an *inactivation* gate respectively, while α(V) and β(V) are the voltage-dependent *rate constants* of the gates, which describe how the "gate" switches between "open" and "close" state. Eq (1.9) is the solution of Eq. (1.5). We omitted the equations of rate constants for the *h* gate, but it will be similar to Eqs. (1.8)-(1.9). In principle, as long as we obtain parameters for rate constants, we can fully model the corresponding ion channel with Eqs. (1.4)-(1.9). However, in practice, if we want to build a new ion channel directly from literatures, there are typically not sufficient information for solving α(V) and β(V) for a particular ion channel. The most common data regarding ion channel kinetics found in literatures are: (1) the steady-state m_∞ of gate variable *m* (or *h*) ; (2) time constant τ_m of *m* (or *h*). These data are often represented as "sparse points" instead of continuous curves. Fitting sparse data with α(V) and β(V) will inevitably bring in unexpected errors. In this regards, GENESIS provides a "short-cut"—"*tabchannel*"object—straight to the Eqs. (1.9) by incorporating m_∞ and τ_m directly taken from experimental data (James M. Bower and Beeman 2003). The "tabchannel" aims to make *tabulated* HH model. Instead of using fitted α(V) and β(V) , it creates a big table and expands the table for m_∞ or τ_m by interpolating on the existed values, i.e. the "sparse" points reported in the literatures.

1.3.4 Reconstructing neuron morphology

If one cannot find desired morphology data at hand, one can always turn to e.g. "NeuroMorpho", the largest on-line database that contains thousands of realistic neuronal morphologies and is fully open to the public (Ascoli, Donohue et al. 2007). Raw data cannot

be imported into GENESIS directly. NeuroMorpho provides both raw data and a software that can "translate" raw data into GENESIS format. Some other software, such as "NeuronML", have similar function. Recently, HBP and Allen institute have released large amount of neuronal morphology data, most of which can be found in HBP its own platforms or in ModelDB.

Morphology data need to be double-checked before it is used for simulations. For instance, dendritic resistance is extremely sensitive to diameters. However, due to measurement or tracing problem, one common problem in the raw morphology data is the inconsistency in thickness of dendrites—they could suddenly go too thin or too thick, which will significantly affect the accuracy of the model and even create artefacts.

1.3.5 Numerical accuracy when simulating complex neuron models

Simulators such as GENESIS adopts a list of numerical method to solve coupled differential equations, including *Forward/Backward/Exponential Euler* method, *Adams-Bashforth* Methods and *Crank-Nicholson* Method (James M. Bower and Beeman 2003). These integration methods allow GENESIS to "approximate" solutions for differential equations at each time step. When the number of differential equations in the system grows large, the numerical accuracy of the system will become "unstable" and critically depends on the size of time-step (James M. Bower and Beeman 2003). To obtain satisfying accuracy, we are forced to use a small time-step, which in turn makes simulations slow.

To achieve a good trade-off between speed and accuracy, the numerical methods must be tested with various time-step. *Crank-Nicholson* Method is an average of *Forward* and *Backward Euler* method (Figure. 2), thus it appears to be a good balance between simulation efficiency and accuracy.

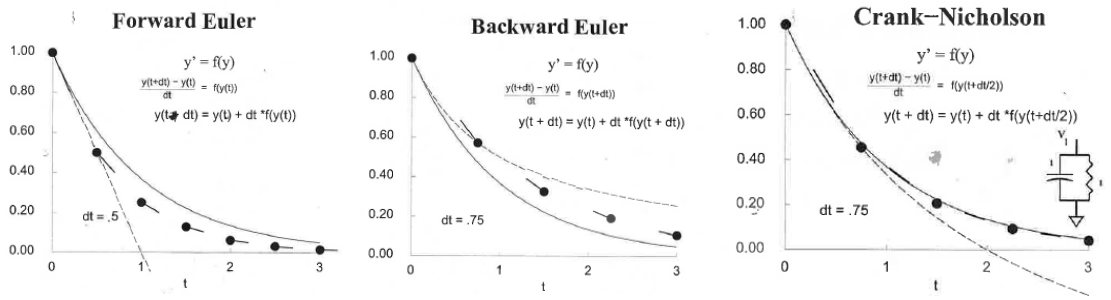

Figure 2. An illustration of *Forward-*, *Backward-*, and *Crank-Nicholson* method. Solid lines are true value while dashed lines are fitted values. "*y(t)"* is the target function and "*dt*" is the time-step used in simulations. Modified from the on-line tutorials of NEURON (https://www.neuron.yale.edu/neuron/courses).

2 AIMS

Neuronal dendrites are capable of performing comprehensive computations. Here we are interested in the principal neurons of the striatum, the medium-spiny neurons (MSNs) which lie at the entrance of basal ganglia and govern the inputs from cortex and thalamus to basal ganglia. The aim of this thesis is to explore how dendrites of MSNs may shape synaptic plasticity, and how interactions between synaptic excitation and inhibition alter the output of MSNs.

The specific aims of the present thesis were:

- To explore possible mechanisms underlying GABA-dependent control of spike timing-dependent plasticity (STDP) polarity in MSNs (paper I).

- To further identify how subunits of NMDARs affect STDP in MSNs (paper II).

- To explore dendritic plateaus in MSNs and their computational significance for synaptic excitation and inhibition (paper III).

3 METHODS

This thesis is a pure computational study, while all animal experiments were performed in our collaborators labs. Although the core of the thesis is to construct biologically "realistic" model for MSNs and use the models to explore synaptic integrations, the presented papers combine computational and experimental approaches. To better understand this work, we will focus on computational methodology, but also summarize experimental background briefly. For all MSN models in this thesis, we do not intend to distinguish D1- or D2-MSN.

3.1 PAPER I

3.1.1 Passive properties in the detailed MSN model

A biophysically detailed model of MSN was developed based on previous published MSN model for ventral striatum (Wolf, Moyer et al. 2005). The previous MSN model (Wolf, Moyer et al. 2005) was coded in the NEURON simulator (Hines and Carnevale 1997), while the current version was implemented in the GENESIS environment (James M. Bower and Beeman 2003). The model parameters were further modified to fit current experiment conditions in dorsal striatum. The main targeted features in this model include: (1) significant inward rectifications when the soma were clamped at negative potential relative to resting membrane potentials (-80 mV in our case). (2) the current-frequency curve of the model matches experimental conditions. (3) TTX-dependent bAPs. (4) More realistic calcium dynamics observed in dendrites.

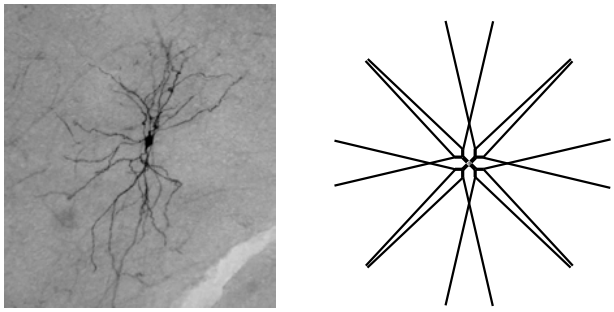

Figure 3. The real morphology of an MSN (left) and its simplified version (right) used in the previous Wolf's model and the models in paper I and II. Taken from Wolf's model (Wolf, Moyer et al. 2005) with permission.

The morphology of the MSN model was the same as in Wolf's model (Wolf, Moyer et al. 2005) (Fig.3). To conclude, the model has four primary dendrites (20 µm each), eight secondary dendrites (24 µm each), and 16 tertiary dendritic branches (each tertiary branch containing 11 compartments of 36 µm). The additional spine areas were compensated by adjusting the morphology data as in previous study (Wolf, Moyer et al. 2005). The input resistance of the current model was tuned to be 210 MΩ (-50 pA somatic current injection at the resting state) in agreement with the experiment conditions in collaborators lab. The other passive parameters include: specific axial resistance, 4 Ω.m in the soma/axon and primary/secondary dendrites, 2 Ω.m in the tertiary dendrites; specific membrane resistance, 8 $\Omega.m^2$ for the whole cell ; E_{leak} = -60 mV ; membrane capacitance C_F, 0.01 F/m^2 .

3.1.2 Active properties in the detailed MSN model

Ion channel types of the model were the same as in the published MSN model (Wolf, Moyer et al. 2005), including: Q-, R-, T-, N-, and L-type (both CaV1.2 and CaV1.3) calcium channels; fast and persistent sodium channels (Naf and NaP), fast (Kv4.2) and slow A-type (Kv1.2) potassium channels (KAf and KAs), inward-rectifier potassium channels (KIR), small-conductance calcium-dependent potassium channels (SK), and large-conductance calcium-dependent potassium channels (BK). The ion channel kinetics were slightly modified based on available literature. We adopted a calcium buffer system other than in Wolf's model (Wolf, Moyer et al. 2005). The new calcium buffer model was taken from experimental measurements of calcium in MSNs (Carter and Sabatini 2004). Using this calcium buffering system, the model can reproduce the dendritic calcium dynamics reported in MSNs (Day, Wokosin et al. 2008). Details regarding the ion channels densities and kinetics can be found in the following tables: Table 1 presents the maximal conductance of non-calcium channels in the model, Table 2 presents the maximal permeability of calcium channels in the model and Table 3 shows the kinetics of all non-calcium ion channels using the HH formalism. The calcium channel kinetics are the same as in Wolf's model (Wolf, Moyer et al. 2005).

Table 1. Maximal conductance of noncalcium channels in the model (S/m^2)

Channel name	Soma	Proximal dendrites	Distal dendrites
Naf	15,000	1560	195
NaP	0.4	1.38e-3	1.38e-3
KAf	2250	630	210
KAs	166.4	15.216	15.216
Kir	4.34	4.34	4.34
Kdr	28	28	28
SK	0.5	0.5	0.5
BK	10	10	10

Table 2. Maximal permeability of calcium channels in the model (m/s)

Channel name	Soma	Proximal dendrites	Distal dendrites
CaQ	3e-7		
CaN	1.05e-7		
CaR	13e-7	13e-7	13e-7
CaV1.2	2.8475e-8	2.8475e-8	2.8475e-8
CaV1.3	2.125e-7	2.125e-7	2.125e-7
CaT	11.75e-9	11.75e-9	11.75e-9

3.1.3 Modeling synaptic inputs

The model contains explicitly modeled spines. We only inserted 10-15 spines into the model without distorting membrane surface of the model. The spine consisted of two cylinder compartments: spine head (length, 1 µm; diameter, 0.5 µm) and spine neck (length, 1 µm; diameter, 0.1 µm). Based on experimental studies (Carter and Sabatini 2004), calcium

channels which were experimentally verified were added onto the spine head which were experimentally identified, including: R-, T-, and L-type ($Ca_V1.3$ and $Ca_V1.2$) calcium channels. NMDA/AMPA channels were also inserted to the spine-head, with the kinetics taken from dorsal striatum (Chapman, Keefe et al. 2003). To keep track on the different calcium resources, we set up two separate calcium buffer pools in the spine head (Wolf, Moyer et al. 2005): "L-type calcium pool" linked to L-type ($Ca_V1.3$ and $Ca_V1.2$) calcium channels; "NMDA calcium pool" coupled to NMDARs and AMPARs. Note in MSNs, a small fraction in the AMPA influx contains calcium currents (Carter and Sabatini 2004). Maximal permeability of calcium channels in the spines (unit: m/s): CaT, 2.35e-8; CaR, 1.3e-6; CaV1.2, 5.695e-8; and CaV1.3, 4.25e-7.

Table 3. Ion channel kinetics

The rates of open gates for the updated channels are given from the equation: value = 1 / (1 + exp [(V – V_{half}) / Slope]). α and β are the rate constants in Eqs. (1.5-1.8).

Channel Name	mh form	Steady State	tau	scale	α or β	Vhalf (mV)	Slope (mV)	Rate
NaF	m^3	sigmoid	tab	1.2	-	−25	−9.2	1
	h	sigmoid	tab	1.2	-	−62	6	1
Kir	m	sigmoid	tab	0.5	-	−102	13	1
KaF	m^2	α/(α+β)	1/(α+β)	1.5	α (sigmoid)	4	−17	1.5 ms^{-1}
					β (sigmoid)	10	9	0.6 ms^{-1}
	h	α/(α+β)	1/(α+β)	0.67	α (sigmoid)	−121	22	105 s^{-1}
					β (sigmoid)	−55	−11	65 s^{-1}
KaS	m^2	α/(α+β)	1/(α+β)	2.5	α (sigmoid)	50	−20	250 s^{-1}
					β (sigmoid)	−90	35	50 s^{-1}
	h	α/(α+β)	1/(α+β)	2.5	α (sigmoid)	−95	16	2.5 s^{-1}
					β (sigmoid)	50	−70	2 s^{-1}
Kdr	m	1/(1+a)	0.05*b/(1−a) s	0.5	a (exp)	−13	9.09	-
					b (exp)	−13	12.5	-
BK	m	α/(α+β)	1/(α+β)	1	α (BK_eqn1)	D = −0.84, K = 0.003, B = 480 s^{-1}		
					β (BK_eqn2)	D = −1, K = 0.009, B = 280 s^{-1}		
SK	m	SK_eqn	4e-3	1	-	*EC50* = 0.57 μM		

The model in paper I contains both tonic and phasic GABAergic inputs. The tonic background GABA was explicitly modeled based on the available experimental data (Ade, Janssen et al. 2008, Santhakumar, Jones et al. 2010). The phasic GABAergic inputs were modeled with the conductance (1,500 pS) based on the experimental conditions in our collaborator's lab that the amplitude of phasic IPSCs were normally ~13-15 pA observed in the soma. Three GABAergic synapses were inserted onto the local dendritic compartment close to the spine and were activated 5ms after the NMDA/AMPA inputs.

The simulation time-step was typically 5 μs for numerical accuracy purpose.

3.1.4 Experimental Background

All animal experiments were performed in our collaboration lab at College de France in accordance with European Union guidelines (directive 86/609/EEC).

In brief, we took horizontal brain slices (330 µm) from OFA rats (P15-P90) of either sex. Patch-recordings were made in physiology conditions (34 C). Solutions in the pipettes (5-8 MΩ) contained (in mM): 105 K-gluconate, 30 KCl (or 127 K-gluconate and 13 KCl for chloride reversal potential E_{Cl} = -60 mV), 10 HEPES, 10 phosphocreatine, 4 ATP-Mg, 0.3 GTP-Na, and 0.3EGTA adjusted to pH7.35 with KOH. The other experimental conditions were the same as in the previous experiment (Fino, Glowinski et al. 2005).

In the STDP protocols, EPSCs (~50-200 pA, "pre") in MSNs were induced by stimulating layer 5 somatosensory cortex with a bipolar electrode. The action potential ("post") was induced by injecting a 30ms step current to the soma of MSNs. The "pre" and "post" signals were coupled with a Δt of -20 to +25 ms and repeated for 150 times at 1Hz.

3.2 PAPER II

3.2.1 Passive and active properties in the detailed MSN model

A "sister" model of the MSN model in paper I was built in this paper. Although all animal experiments in paper I and II were performed by the same collaborator lab, they were designed as separated experiments. MSNs recorded in these two papers might vary. Therefore, despite the current model has identical morphology, ion channel types and calcium buffer as the model in paper I, we had to retune the model parameters to fit experiment conditions such as current-frequency curves in this paper. The difference between these two models might reflect variations in individual MSN physiology. Detailed ion channel distributions are as Table 4:

Table 4: ion channel distributions in the MSN model

Gbar (S/M^2)	soma	prox dend	mid dend	dist dend	spine
NaF	90,000	2,730	2,730	975	0
KaF	765.24	765.24	168.21	112.14	0
KaS	360.1	38.93	38.93	38.93	0
Kir	8	8	8	8	0
KDR	6.04	6.04	6.04	6.04	0
SK	2	2	2	2	0
BK	10	10	10	10	0
Pbar					
CaL1.3	1.59E-07	1.59E-07	1.59E-07	1.59E-07	4.25E-07
CaT	8.81E-09	8.81E-09	8.81E-09	8.81E-09	2.35E-08
CaR	9.75E-07	9.75E-07	9.75E-07	9.75E-07	1.30E-06
CaN	3.75E-07	3.75E-07	3.75E-07	3.75E-07	0
CaL1.2	1.26E-07	1.26E-07	1.26E-07	1.26E-07	3.35E-07

Gbar = maximal conductance S/M^2 = Siemans per meter squared;
Pbar = maximal calcium permeability. Prox dend = proximal dendrites; mid dend = middle dendrites; dist dend = distal dendrites.

3.2.2 Modeling synaptic inputs

To model different subunits of NMDARs, we took the classic double-exponential (τ_{rise} and τ_{decay}) model (Eqs. 1.1-1.3) , while varying values of τ_{decay} and "1/ ŋ " in the Eq. 1.3 for "Mg^{2+} block" according to experiment data (Laurie and Seeburg 1994, Monyer, Burnashev et al. 1994, Vicini, Wang et al. 1998). Details of the NMDA subunits parameters can be found in the Table 5:

Table 5: NMDAR subunits parameters

	GluN2A	GluN2B	GluN2C	GluN2D
Gmax (S)	0.94e-9	0.94e-9	0.325e-9	0.119e-9
Tau decay (s)	25e-3	150e-3	125e-3	850e-3
Mg^{2+} block	3.57	3.57	25	40

3.2.3 Experimental background

Animal experiments were performed by our collaboration lab as in paper I. All experiment protocols were the same as in paper I except Picrotoxin (50 µM) were added in the external solutions throughout all experiments.

3.3 PAPER III

In this study, we constructed a new MSN model different from the models used in paper I and II. The major differences are: (1) we used morphology data from a real MSN, instead of using simplified morphological patterns in paper I and II. Using more realistic morphology might help to capture subtle details of synaptic integration in distal dendrites of MSNs. (2) ion channels densities in the dendrites were tuned to produce non-linear integration properties such as dendritic plateaus.

3.3.1 Passive properties of the detailed MSN model

We choose morphology data of a real MSN from the public database "NeuroMorpho" (Ascoli, Donohue et al. 2007) (cell ID, NMO_04520). The original data had 2,014 compartments and consisted of 15 primary stems, 59 bifurcations and 133 branches with total dendritic length of 2,470 µm. To reduce the computing cost, we merged small "segments" in the original data into longer segments (Lindroos, Pieczkowski et al. 2015). Thus, we obtained a new model of 634 compartments but without altering its three-dimensional structure, which has identical dendritic length and patterns as in the original data (Lindroos, Pieczkowski et al. 2015).

To account for additional surface due to a great number of spines, we used an theoretical formula to adjust dendritic length (l) and diameters (d) (Wolf, Moyer et al. 2005):

$$L = l * F^{\frac{2}{3}}$$

$$D = d * F^{\frac{1}{3}}$$

Here *L* and *D* stands for adjusted length and diameter. "F" is an empirical factor. To precisely obtain the "F" factor for the current model, we designed two MSN models (634 compartments) with identical morphology and passive properties: one model was covered by passive spines uniformly distributed from 30 µm from the soma (1 spine / µm), while the second model had no spines but only using "F" factors to adjust their dendritic length and diameters. We manually tuned "F" factor in the second model to match its output to the first model. In such way, we found F = 1.38 was the best value in this study. The other passive parameters in the model were: specific axial resistance at 4 Ωm, specific membrane resistance at 1.8 Ωm^2, reversal potential of leak channels at −-70 mV, and membrane capacitance at 0.01 F/m^2.

3.3.2 Active properties of the detailed MSN model

The model contains a large array of ion channels, most of which were the same as in Paper I and II, including: fast sodium channels (NAf), fast and slow A-type potassium channels (KAf and KAs), Inward-Rectified potassium channels (Kir2), Delayed-rectified potassium channels (Kdr), T-type ($Ca_v3.2$,$Ca_v3.3$), L-type ($Ca_v1.2$, $Ca_v1.3$) and R-type ($Ca_v2.3$) calcium channels, and calcium-activated potassium channels (SK and BK). The newly introduced ion channels were two subtypes of T-type calcium channels (Iftinca, Mckay et al. 2006): $Ca_v3.2$ and $Ca_v3.3$. Note that the $Ca_v3.3$, a unique subtype with very slow inactivation time constant (~100 ms) (Iftinca, Mckay et al. 2006), was abundant in the striatum (Yunker, Sharp et al. 2003). The ion channels kinetics were slightly modified from those in paper I and II. In particular, the channel conductance, q-factors that account for temperature effects on ion channel kinetics and distribution were tuned to fit current experimental conditions in our collaborator's lab at Stanford for this study. The calcium buffer was identical to those in paper I and II. All simulations were presumed to be near physiology temperature (~32 ºC).

Details of ion channels can be found in the table 6-8:

Table 6: Maximal conductance of non-calcium channels in the model (S/m^2)

name	soma/axon	proximal dendrite	distal dendrite
NaF	108000	292.5	97.5
NaP	0.4	0.4	0.4
KaF	5785.2	562.5	375
KaS	554	22.9	22.9
Kir	16.8	12.6	12.6

Kdr	21.75	7.25	7.25
Sk	10	10	10
Bk	500	150	150

Table 7: Maximal permeability of calcium channels in the model (m/s)

name	soma/axon	proximal dendrite	distal dendrite	spine
N-type	5.00E-07			
R-type	6.50E-07	6.50E-07	6.50E-07	7.80E-07
$Ca_v3.2$, T-type			1.76E-09	9.40E-09
$Ca_v3.3$, T-type			1.76E-09	2.35E-08
$Ca_v1.2$, L-type	8.38E-08	8.38E-08	8.38E-08	
$Ca_v1.3$, L-type	1.06E-08	1.06E-08	1.06E-08	

Table 8: Ion channel kinetics summary

The table includes: (1) Experimental references for ion channels and (2) main channel differences from the models in paper I and II. The rates of open gates for the updated channels are given from the equation: value = 1 / (1 + exp [(V – V_{half}) / Slope])

Name	Reference	Scale factor	Gate	Tau (ms)	Vhalf (mV)	Slope (mV)
$Ca_v3.3$	(Iftinca et al., 2006)	3/2	m^2	table	-78.01	-5.472
		3	h	table	-78.3	6.5
$Ca_v3.2$	(Iftinca et al., 2006)	3	m	table	-37.9	-6.2
		3	h	table	-59.2	8.8
CaR	(Foehring et al., 2000)	1	m^3	1.7	-8.46	-25.98
		3	h			
KaS	(Shen et al., 2004)	2.8	m^2			
		2.8	h	$1/[(\alpha\alpha+\beta)*0.6 + 0.4]$		
KaF	(Tkatch et al., 2000)	1				
		2				
NaF	(Nobukuni Ogata and Tatebayashi, 1990)	2				
		2				
Kdr	(Migliore et al., 1999)	3				
Kir	(Steephen and Manchanda, 2009)	same as in our previous model (Evans et al., 2012)				
CaN	(Kasai and Neher, 1992; Churchill and Macvicar, 1998; McNaughton and Randall, 1997)					
$Ca_v1.2$	(Kasai and Neher, 1992; Churchill and Macvicar, 1998; Bell et al., 2001)					

$Ca_v1.3$	(Kasai and Neher, 1992; Bell et al., 2001; Xu and Lipscombe, 2001)	
SK	(Maylie et al., 2004)	
NaP	(Magistretti and Alonso, 1999)	same as in our previous model (Paille et al., 2013)
BK	(Moczydlowski and Latorre, 1983)	

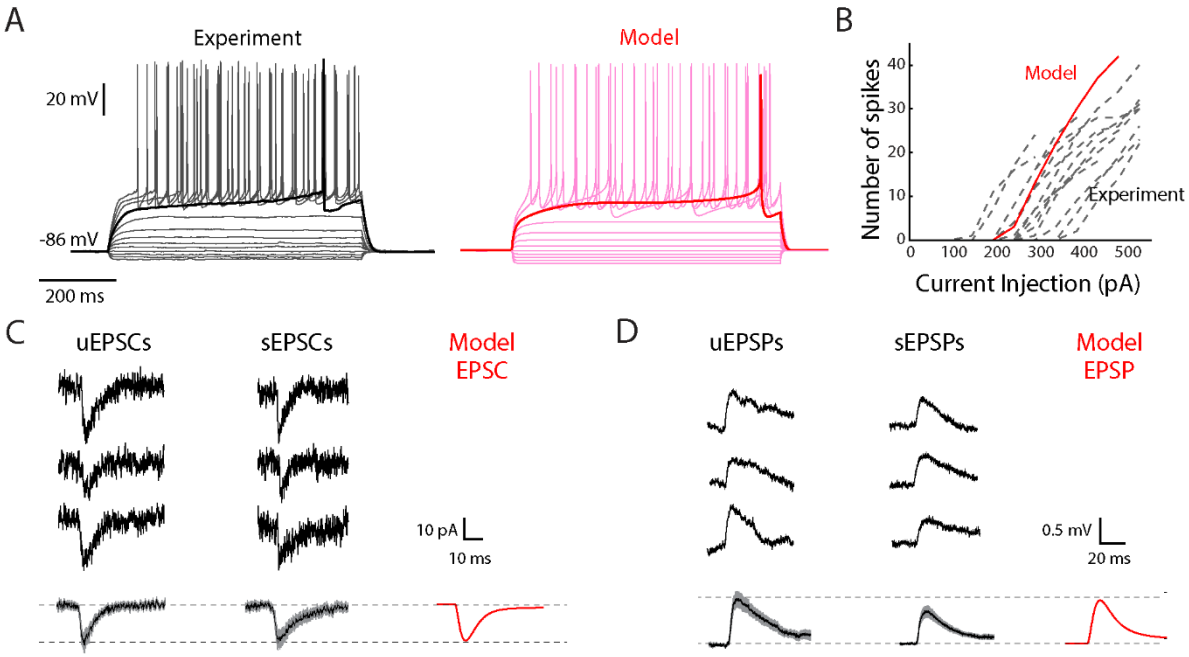

Figure 4 Comparing model outputs with experiment data. ***A***, voltage traces in response to step current injections. ***B***, Injection-Frequency curves. Dashed lines are the curves obtained from a group of MSNs in this study. ***C-D,*** Comparison of EPSCs and EPSPs between the model and experiment data.

3.3.3 Modeling synaptic inputs

In this section I will introduce how to model synapses and how to design random input patterns.

Synaptic receptors

The model contains $GABA_A$, AMPA and NMDA receptors. We follow the same formalism to model the receptors as in paper I and II. In brief, the conventional "dual exponential" function was adopted to model synaptic channel kinetics and implemented with the "*synchan*" object in GENESIS (James M. Bower and Beeman 2003) . For $GABA_A$ and AMPA channels, their conductance function Gk was modeled by:

$$Gk(t) = \frac{A * gmax}{\tau 1 - \tau 2} \left(e^{-\frac{t}{\tau 1}} - e^{-\frac{t}{\tau 2}}\right)$$

By varying τ1 and τ2, we were able to model different types of GABAergic inputs onto MSNs, including collateral inhibitions from neighboring MSNs, somatic inhibition from fast-spiking interneurons and slow-$GABA_A$ inhibition likely from NPY-NGF interneurons, etc.

NMDA receptors were modeled by adding additional "Mg-block" effects:

$$f_{Mg\_block} = \frac{1}{1+\eta[Mg^{2+}]e^{-rV}}$$

$[Mg^{2+}]$ = 1 (mM), ŋ = 2.992, r = 0.01369 (Vargas-Caballero and Robinson 2003)

Details of modeling different types of synaptic channels can be found in the table 9:

Table 9: synaptic receptor kinetics

Synaptic channel type	τ_1 (ms)	τ_2 (ms)	Erev (mV)
Collateral inhibition (Taverna, Ilijic et al. 2008)	1	10	- 60
Somatic FS inhibition (Galarreta and Hestrin 1997)	0.25	3.75	- 60
Slow $GABA_A$ Receptor (Ibanez-Sandoval, Tecuapetla et al. 2011)	10	80	- 60
NMDA Receptor (Chapman, Keefe et al. 2003)	5.63/2	231/2	0
AMPA Receptor (Ding, Peterson et al. 2008)	1.9	4.8	0

We placed NMDA/AMPA receptors on both spine heads and dendrites. NMDA/AMPA receptors on spine heads used g_{max}NMDA = 1880 pS, g_{max}AMPA = 340 pS, while the NMDA/AMPA receptors on dendrites were g_{max}NMDA = 705 pS, g_{max}AMPA = 255 pS, respectively. The amplitude of single EPSP recorded in the soma was from ~0.5 mV to ~0.8 mV. The maximal conductance of all unitary GABAergic synapses were 1,500 pS, which are in the range as previously reported and match our experiment observations (Planert, Szydlowski et al. 2010, Ibanez-Sandoval, Tecuapetla et al. 2011).

Modeling Spontaneous Synaptic Activities

The model has 400 excitatory synapses (g_{max}NMDA = 705 pS, g_{max}AMPA = 255 pS) and 100 GABAergic synapses (g_{max}GABA = 1,500 pS), which is consistent with published data that the ratio between excitatory and inhibitory synapses is approximately 4:1 (Wilson 2007). All spontaneous synapses were randomly distributed over the whole cell and were activated at 1 Hz for excitatory synapse and 0.5 Hz for inhibitory synapses. The spontaneous synaptic activity could elevate the membrane potential from the resting -86 mV to approx. -78 mV. The model is pre-run for 500 ms before inducing a plateau.

Modeling High Frequency Excitatory Inputs

To resemble specific cortical inputs to MSNs (Matyas, Sreenivasan et al. 2010), we modeled a group of 20 NMDA/AMPA synaptic channels (g_{max}NMDA = 705 pS, g_{max}AMPA = 255 pS; independent Poisson trains, 10 Hz ; duration, 200 ms). We generated 1,000 groups of spatial patterns with the following procedure:

- We first generated a large sample pool consisting of 100,000 random spatial patterns (left panel in Figure 5). In each pattern, all synapses were randomly distributed throughout the whole dendritic tree except in the terminal branch receiving the clustered inputs.
- We plotted histograms as functions of the averaged distance to soma (along dendritic path) of 20 synapses.
- Then we randomly picked 1,000 patterns (right panel in Figure 5) from the pool which followed *uniform distribution* in their distribution histogram (100 samples per bin, 10 bins).

During each trial, we used distinct spatial patterns (from the selected 1,000 spatial patterns) and temporal patterns for the excitatory inputs.

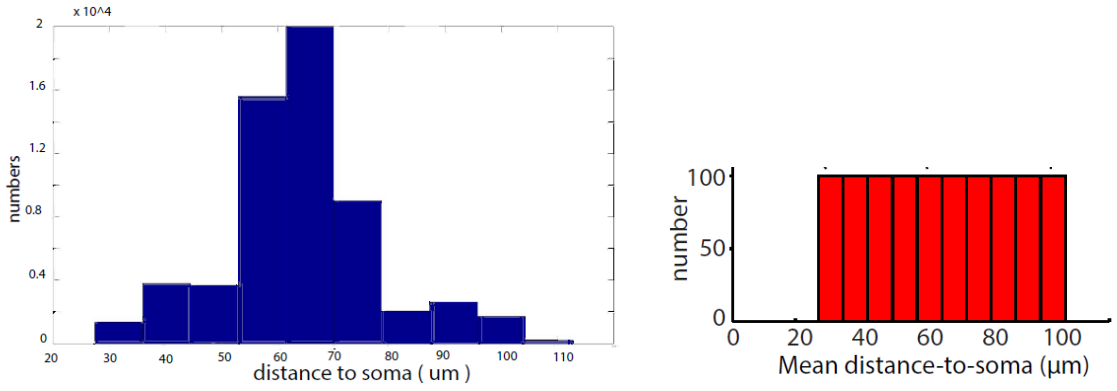

Figure 5 summary of designed spatial patterns for 20 excitatory synapses. ***Left***, histogram of a total 100,000 samples plotted as function of average distance along dendrite (of the 20 synapses) to the soma. ***Right***, histogram of 1,000 selected samples from (**A**). Note the uniform distribution of the spatial patterns.

Modeling somatic inhibitory input trains

The somatic inhibitory trains aimed to mimic inputs from FSIs (independent Poisson trains, 30 Hz for 200 ms), which were exclusively targeted on the perisomatic region. The short-term plasticity with depression was included in the simulated FSI inputs, in accordance with (Planert, Szydlowski et al. 2010).

Random pattern generation in the simulations

We used the "*timetable*" object in GENESIS to create all Poisson trains in our simulations. The generated Poisson trains were exported to files and documented in order to be back-tracked.

Simulation platform and numerical accuracy

Both GENESIS (version 2.3) and PGENESIS were used as the main simulation platforms running in the Unix/Linux environment (Bower and Beeman 1998) . In particular, the PGENESIS was used for simulations with large-scale sample size and run on a super-computer (Clay X30, ~4,000 CPUs) at PDC, KTH Royal Institute of Technology. "*Crank-Nicolson*" (second order) method (Bower and Beeman 1998) was adopted throughout our simulations. We found high precision of running simulations even with a time step of 20-50 μs, which was almost identical to precision of running the same simulations with 1 μs. Therefore, we used 20 μs (for simulation without random inputs) and 50 μs (for simulations with random synaptic inputs) as "time-step" in our simulations.

3.3.4 Experimental background

All animal experiments were performed by our collaboration lab at Stanford University and approved by Stanford University's Administrative Panel on Laboratory Animal Care.

We used adult (5-8 weeks) C56BL6/J mice in this study. Oblique horizontal brain slices (300 μm) containing the dorsal striatum were obtained from mice of both gender as previous described (Wu, Kim et al. 2015). Electrophysiological recordings were performed at near physiology temperature (30 - 31°C). The internal solution in the electrode contained: 135 mM KCH_3SO_3, 5 mM KCl, 10 mM HEPES, 8 mM Na_2-Phosphocreatine, 0.3 mM Na_2GTP, 4 mM MgATP, 0.1 mM $CaCl_2$, 1 mM EGTA (pH 7.2-7.3, 285-290 mOsm). For voltage clamp and dual color experiments, 2 mM QX-314 Cl was added to the internal solution to prevent spiking. Two-photon uncaging of DNI-Glu and single-photon Rubi-GABA were carried out using two different lasers tuned to 730 nm and 450 nm respectively.

4 RESULTS AND DISCUSSION

In this thesis, three projects were performed to explore how dendrites may affect synaptic plasticity and synaptic integration in striatal MSNs.

4.1 GABA CONTROLS THE POLARITY OF SPIKE TIMING-DEPENDENT PLASTICITY (STDP) IN THE STRIATUM (PAPER I)

Spike timing-dependent plasticity is, as explained, a plasticity rule relying on the relative timing between the pre- (i.e. activation of AMPA/NMDA receptors) and post-synaptic (i.e. bAPs) signals (Caporale and Dan 2008). In previous published experiments without GABA blockers, a potent and reliable STDP rule, the 'anti-Hebbian' rule at corticostriatal synapses was found in MSNs (Fino, Glowinski et al. 2005), which is apparently opposite to the finding of 'Hebbian learning' rules at corticostriatal synapses in presence of GABA blockers (Shen, Flajolet et al. 2008). In this study, we aim to investigate the role of GABA in regulating STDP rules in the striatum.

4.1.1 Inhibition of $GABA_A$Rs reverses STDP polarity at corticostriatal synapses

In control conditions (here defined as when $GABA_A$Rs were not pharmacological inhibited in slices), our collaborators observed a robust anti-hebbian plasticity rules at corticostriatal synapses in MSNs: post-pre pairing induced LTP while pre-post pairing induced LTD (Fino, Glowinski et al. 2005). To determine if GABA affects the STDP rules, paired patch-clamp recordings were done on two neighboring MSNs: one MSN was recorded in control conditions, while the other MSN was recorded with PTX inside the pipette (i-PTX) such that GABA effects can be restricted to the postsynaptic neuron solely (Figure 6A). Surprisingly, When the STDP protocols were applied to these two MSNs respectively, it was found that inhibiting $GABA_A$Rs reversed the STDP rule from anti-Hebbian to Hebbian in the MSN loaded with i-PTX: post-pre pairing induced tLTD while pre-post paring induced tLTP (Figure 6B). By contrast, the MSN in the control condition still produced anti-Hebbian learning rule (Figure 6B) as previously reported (Fino, Glowinski et al. 2005).

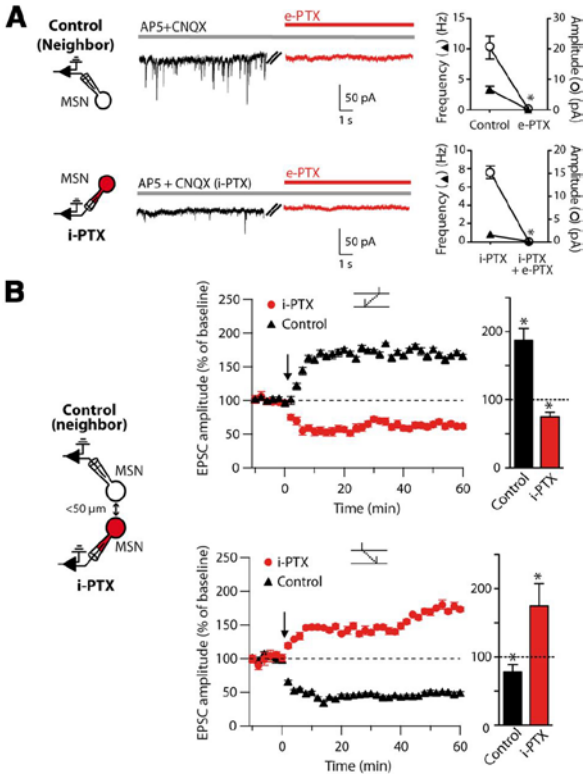

Figure 6 GABA effects on the specific post-synaptic neuron were sufficient to reverse the polarity of STDP. ***A***, sample traces for paired recordings on two neighboring MSNs in the presence or absence of external GABA blocker (e-PTX): one MSN loaded with normal intracellular solution ('control', top trace), another MSN was loaded with intracellular PTX ('i-PTX', 1mM, bottom trace). Right panels, frequency of IPSCs in the presence or absence of external GABA blocker. Note both i-PTX and e-PTX could thus efficiently block $GABA_A$Rs. ***B***, paired recording on two neighboring MSNs (< 50µm) investigated with the STDP protocols. Post-pre paring induced tLTP in the MSN in the control condition while induced tLTD in the MSN loaded with i-PTX (top trace). In contrast, pre-post paring induced tLTD in the MSN in the 'control' condition and tLTP in the MSN loaded with i-PTX (bottom trace).

4.1.2 Model predicts that GABA has a depolarizing effect during the STDP protocols

The plasticity formation likely involved synapses distal in MSN dendrites. To explore dendritic events, we built a biophysically detailed MSN model based on a previously published MSN model (Wolf, Moyer et al. 2005). The model contained a large array of ion channels and was further tuned to fit the experiment conditions when applying the STDP paradigm as well as some new features from more recently published data (Figure 7A-D). The model could reproduce electrophysiological data (Figure 7A-B) as well as the dendritic calcium build up (Figure 7C-D) as in real MSNs. We tried to apply the same STDP protocols to the MSN model as that used in the experiments. Here we included GABAergic inputs right after the 'pre' signals (Figure 7E) based on the assumption that the input also activated e.g. FSIs. Unexpectedly, the model predicted that the GABA depolarized the local dendrite,

instead of counteracting the signals (Figure 7E). Moreover, although the depolarizing effects were potent locally, they could hardly be observed in the soma (dashed lines in Figure 7E).

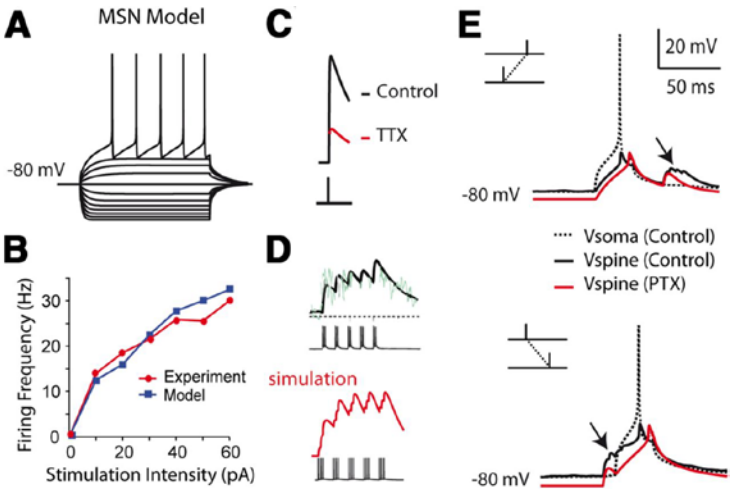

Figure 7. Biophysical model predicts a depolarizing effect of GABA. ***A***–***D***, Model validation. ***A***, Simulated voltage trace in the soma during current step injections. ***B***, Current-firing frequency relationship for an example MSN and for the model MSN. ***C***, Simulated calcium transients recorded in the proximal dendrites (40 – 60 µm from the soma) before and after simulated TTX application. ***D***, Simulated calcium transients in the proximal dendrites (50 – 60 µm from the soma) caused by a spike train (theta burst). The simulated calcium transient trace (red curve) matches the original experimental curve (black curve). ***E***, Simulation of voltage sample traces during post-pre and pre-post STDP pairings. GABAergic inputs depolarize the membrane locally during post-pre and pre-post pairings (black arrows). The spine in the model is located 130 µm from the soma.

4.1.3 The depolarizing effect of GABA may be due to the physiological Cl^- reversal potential

Based on the model prediction that GABA could give a clear depolarizing effect, we wanted to see if this could be supported in the experiments as well. The depolarizing effects of GABA can be attributed to the difference between the resting mean potential (RMP) of MSNs and the reversal potential of $GABA_A$Rs. To determine the reversal potential for $GABA_A$Rs, cell-attached recordings on MSNs were performed, leaving the intracellular environment of MSNs as intact as possible. Then E_{GABA} was estimated via recorded i_{NMDA} and i_{GABA} (Figure 8). The results indicated a driving force of $GABA_A$Rs was 17.2 ± 7 mV from the measured RMP (-78 mV) and E_{GABA} = -60.8 mV (Figure 8). The measurements were thus consistent with the model prediction of GABA depolarizing effects.

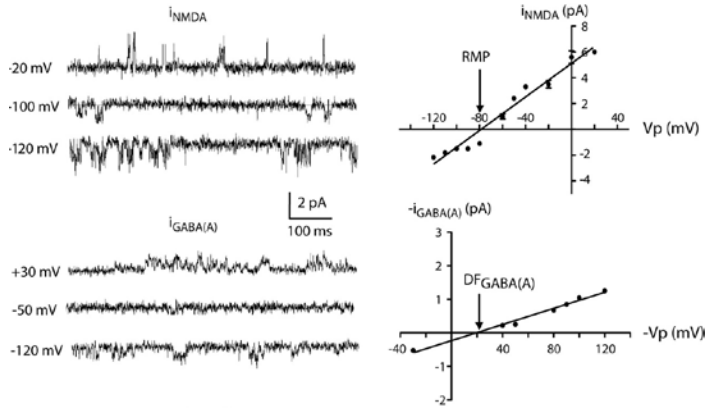

Figure 8. Recordings of unitary NMDA currents (top traces) and GABA currents (bottom traces) at various holding potentials. GABA currents were obtained by cell-attached recordings. RMP is determined at the value indicated by the arrow on the graph. The driving force of chloride ions (DF_{GABA}) through GABAARs is determined at the value indicated by the arrow via the equation: $E_{GABA} = DF_{GABA} + RMP$.

4.1.4 The STDP induction requires different signaling pathways

It was reported that tLTP is dependent on NMDAR activation and tLTD relies on type-1 cannabinoid receptor (CB1R) activation for STDP induction at cortostriatal synapses (Shen, Flajolet et al. 2008). However, this conclusion was made in the condition that $GABA_A$Rs were pharmaceutically blocked (Shen, Flajolet et al. 2008). We therefore asked if the presence of GABA would affect the role of these pathways. Interestingly, we found the signaling pathways for STDP inductions were similar in control and $GABA_A$R blockade conditions (Figure 9). When $GABA_A$Rs were generally blocked by PTX, tLTP induced by pre-post paring required NMDAR activation and tLTD induced by post-pre pairing required activation of CB1Rs, in consistent with previous reported results (Shen, Flajolet et al. 2008). In control conditions, where GABAergic inputs were left intact, the tLTP induced by post-pre paring also required activation of NMDARs and the tLTD induced by pre-post pairing required CB1R activations. It thus appears that the presence of GABA doesn't altered the signaling pathways for STDP inductions.

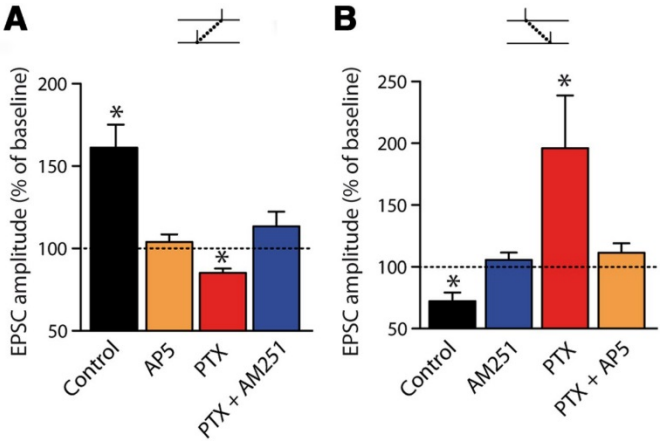

Figure 9. Pharmacology of post-pre (***A***) and pore-post paring (***B***) in control and GABA blockade conditions. AP5 is an NMDAR blocker and AM251 is a CB1R blocker.

4.1.5 Model predicts that depolarization by GABA alters the balance between different signaling pathways underlying STDP induction

If GABA doesn't change the signaling pathways underlying STDP induction at corticostriatal synapses, one plausible explanation is the presence of GABA might alter the balance between these pathways. It has been known that NMDAR-mediated calcium elevations are necessary for LTP formation (Shen, Flajolet et al. 2008), whereas endocannabinoid signaling via L-type VSCC activation (Shen, Flajolet et al. 2008), in particular $Ca_V1.3$ (low-voltage gated L-type VSCC) (Olson, Tkatch et al. 2005) are important for LTD formation. We therefore used the model to explore the dynamics of NMDAR-mediated calcium and L-type calcium during the STDP protocols. The model predicted that due to its depolarization effects, the GABAergic input boosts both NMDAR-mediated calcium and L-type calcium in the dendrites (Figure 10A-B), suggesting that perhaps a competition goes on between tLTD and tLTP formation and different calcium sources might alter the outcome. Finally, we investigated how successively increasing GABAergic inputs in the model influenced the balance between NMDAR and L-type VSCC-dependent calcium influxes. We found that during post-pre parings, the GABAergic input increased the ratio towards the NMDA calcium that favors LTP formation (Figure 10C); by contrast, during the pre-post pairings, the GABAergic input deceased the ratio towards L-type calcium that more favors LTD formation. Increasing GABAergic inputs strengthened these trends consistently. In brief, the model predicted that presence of GABA altered the balance between different calcium resources during the STDP protocols.

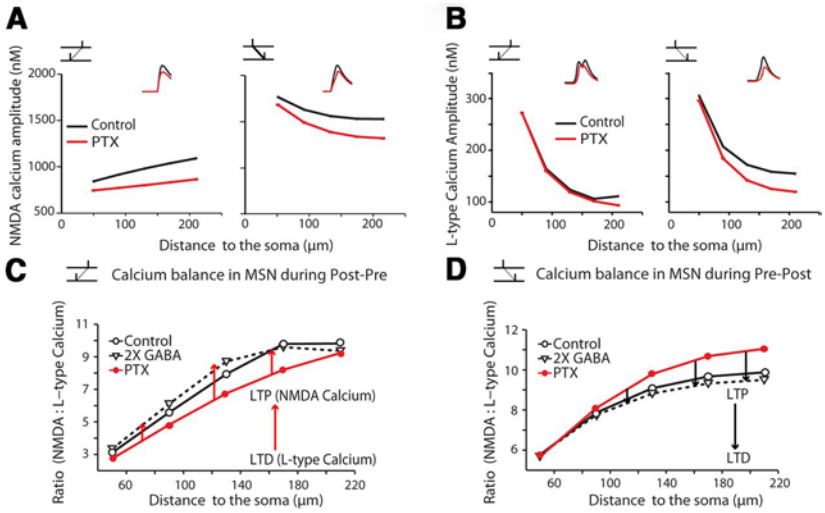

Figure 10. Model predicted GABA effects on L-type voltage-sensitive calcium channels (VSCC) - and NMDAR-dependent calcium influxes. ***A***-***B***, Simulated distributions of NMDAR-dependent (***A***) and L-type VSCC-dependent (***B***) calcium elevations along the dendrites during STDP protocols (*n* = 15). Results are mean values of the MSN model (n=15). Insets: Example calcium traces. ***C***-***D***, Ratio/balance between simulated NMDAR and L-type VSCC calcium (*n* = 15) during post-pre (***C***) or

pre-post (***D***) parings. Arrows indicate the moving direction of the balance between NMDA- and L-type calcium with successively increasing strength of GABA inputs.

4.1.6 Discussions – paper I

GABAergic neurons are known to modulate the spike timing in many brain regions. It is not known how GABAergic inputs modulate synaptic plasticity. In the striatum, corticostriatal synapses in MSNs were reported to present an anti-Hebbian learning rule when GABAergic inputs were kept intact (Fino, Glowinski et al. 2005), in contrast to previous reported Hebbian-learning rule in the striatum with $GABA_A$Rs pharmaceutically inhibited (Shen, Flajolet et al. 2008). In this study, we therefore investigated the impact of $GABA_A$Rs on the STDP rule in striatal MSNs. We found that the presence of GABA could reverse the polarity of the STDP at corticostriatal synapses in MSNs, i.e. changing it from 'anti-Hebbian' to 'Hebbian'. The model predicted that GABAergic inputs coupled to the STDP protocol used in our collaborator's lab depolarized distal dendrites, which further altered the balance of NMDA-mediated calcium (leading to LTP formation) and L-type calcium (leading to LTD formation). This correlation in the model is intriguing and can stimulate further hypotheses to be tested in experiments under different conditions. In the model we also varied different conditions to see what could affect the relative role of GABA and found that e.g. the assumption of the GABA reversal potential, the resting state level, and the timing of GABA inputs could influence the results. Since factors such as these might vary during *in vivo* conditions or between different in vitro paradigms, the outcomes may vary. Interestingly, our findings of an anti-Hebbian learning rule similar to *in vivo* recordings of STDP at corticostriatal synapses (Schulz, Redgrave et al. 2010), where they compared slopes of EPSPs before and after the STDP protocol.

The anti-Hebbian learning rule may help to detect novel cortical pattern and improve action selections in some way. Theoretical studies have for instance suggested that the anti-Hebbian rules could decorrelate the association between frequent patterns and favor selections for infrequent patterns (Roberts and Leen 2010). *In vivo* calcium imaging data have revealed that during sensory control of motor functions, a 'hotspot' in the sensory cortex gave rise to broad activation of entire motor and sensory cortex (Matyas, Sreenivasan et al. 2010). Any novel sensory pattern could be 'drawn' from these massive activation of cortex. When all these cortical activities are projected to the striatum, anti-Hebbian plasticity perhaps could first decorrelate sequentially activated patterns and allow novel patterns to be easily detected.

It should of course also be noted that there exist alternative explanations to the achieved experimental results. In *in vitro* slice experiments an ongoing neuromodulation present in *in vivo* situations may be lacking or altered. For example it is not known how dopamine, acetylcholine, adenosine levels differed between the pre-post and post-pre inputs used. Timing between such inputs might significantly change the outcome (Yagishita, Hayashi-Takagi et al. 2014, Nair, Gutierrez-Arenas et al. 2015, Nair, Bhalla et al. 2016). One should also acknowledge that the 'resting state' might not be representative of *in vivo* conditions, etc.

Finally, although the outcome in terms of LTP or LTD might be different in other experimental or *in vivo* conditions, the observation that i-PTX could alter the balance between LTP and LTD in intriguing and suggest that perhaps there are some completion going on between intracellular processes leading to LTP and LTD. For example it might be the case that signaling known to promote LTP can counteract the processes leading to LTD. For instance PKA can counteract the Gq signaling needed for endocannabinoid production (Shen, Plotkin et al. 2016) and also CaMKII activation might do a similar thing by inhibiting steps further down the cascade leading to endocannabinoid production (Shonesy, Wang et al. 2013). If LTP and LTD processes compete it is indeed possible that a shift in the balance of calcium, cAMP, or some resulting balance in kinases and phosphatases could be amplified and affect the result. It will be a challenge to entangle such factors and understand how they affect synaptic plasticity during *in vivo* conditions.

4.2 THE EFFECTS OF NMDA SUBUNITS ON STDP (PAPER II)

Long-term potentiation in MSNs (LTP) relies, as already said, on NMDAR-mediated calcium influx (Shen, Flajolet et al. 2008). It has been reported that GluN2A and GluN2B subunits are abundant in the striatum (Chapman, Keefe et al. 2003). Interestingly, in Parkinson's disease model, the subunits of NMDARs in the striatum are altered (Nash and Brotchie 2002). However, it was not well understood how subunits of NMDARs would affect the STDP in the striatum. In this study, we aim to investigate how GluN2 subunits impact on tLTP. Can small changes in calcium influx and calcium dynamics, which are expected to be a bit different for different compositions of the NMDA receptor, be detected and give rise to different outcomes? In this study we used modeling to compare how different the calcium influx might be and then compared with experiments in our collaborator's lab.

4.2.1 NMDAR-mediated calcium elevation is predicted to depend on the GluN2 subunits during the STDP protocol

To explore the NMDAR-mediated calcium dynamics during the pre-post paring as in paper I, we used our biophysically detailed model of MSN again. The model in this study is a 'sister' model to the model built in paper I (same morphology and ion channel types). The ion channel densities were tuned to fit experiment conditions in this paper (Figure 11A-B). Also GABA was blocked during all STDP experiments. The GluN2 subunits (including GluN2A,2B,2C and 2D) differ in their decay time constants and Mg^{2+} affinities (table 2 in Method) and the model was tuned to reproduce this. During the pre-post paring (tLTP) as in paper I, NMDARs were assumed to consist of two GluN1 subunits and two GluN2 subunits (either types of A,B,C and D). tLTP enhanced calcium influx for all GluN2 subunits. In particular, the GluN2A and 2B subunits have highest elevation in normalized peak calcium

(increased more than 250-300%, Figure 11C). Interestingly, the calcium curve of 2B subunit is broader than 2A, suggesting a wider timing-window for tLTP induction.

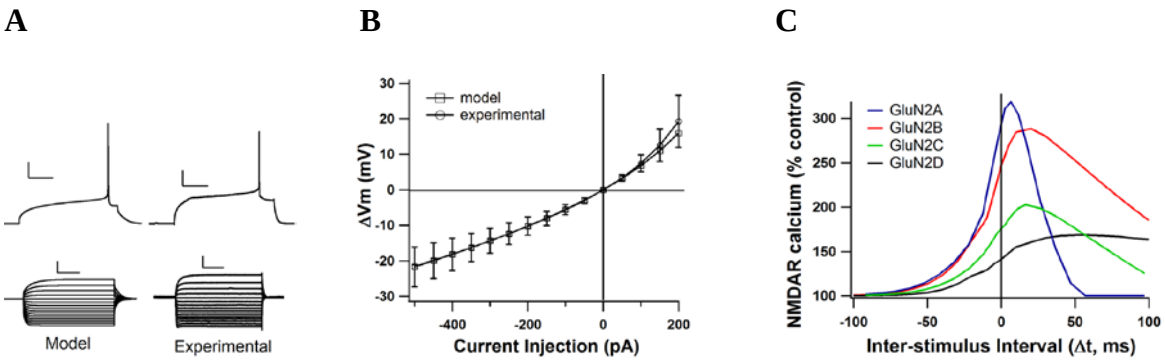

Figure 11. Biophysically detailed model predicted calcium dynamics for GluN2 subunits. **(*A*)** Model membrane voltage traces in responding to step current currents injections. The traces were compared to sample traces measured from one MSN in this study. (***B***) current-voltage relationship of the model compared to experiment data taken from 25 MSNs in dorsal striatum. (***C***) Normalized NMDA-mediated calcium curves with different GluN2 subunits, plotted as functions of Δt between pre and post signals during the pre-post coupling.

4.2.2 NR2B broadens the STDP timing windows

To demonstrate if GluN2A and GluN2B have different timing-window during the STDP protocol, we performed STDP experiments in normal condition ('control', but here with GABA blocked) or in presence of ifenprodil, a selective antagonist of GluN2B. NMDARs in the striatum generally contain both GluN2A and GluN2B subunits (Chapman, Keefe et al. 2003). We first coupled the pre- and post-synaptic signals with a narrow Δt (5 ms<Δt<12 ms). We found that whether we blocked GluN2B or not, the tLTP could always be induced (Figure 12A,C-D). However, if we coupled the pre- and post-synaptic signals with a wider Δt (12 ms<Δt<30 ms), blocking GluN2B (with only GluN2A left) we failed to induce tLTP (Figure 12B-D). Taken together, our experiments confirm that GluN2B subunit broadens the timing-window for tLTP induction.

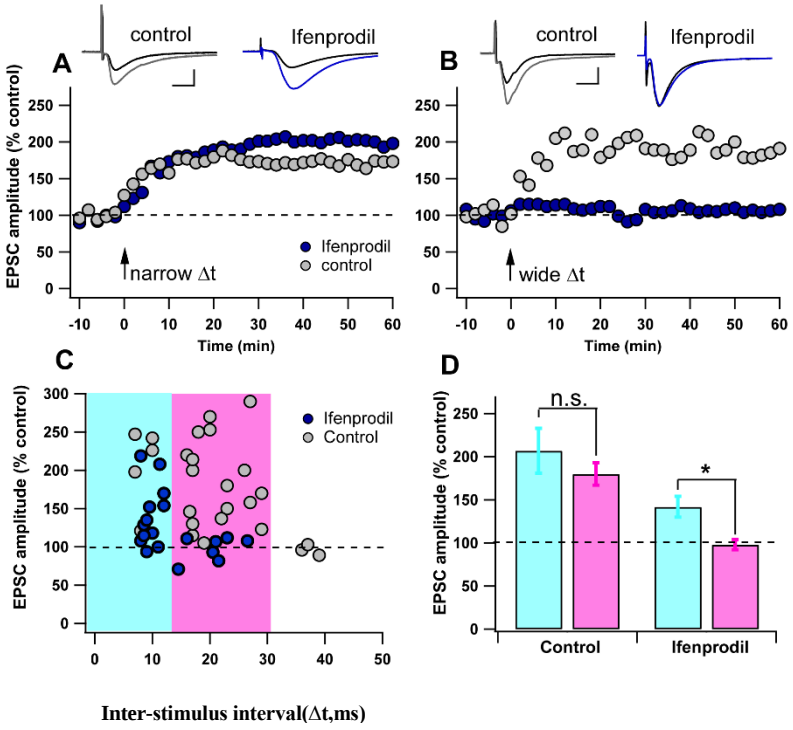

Figure 12. GluN2B broadens the STDP timing window. ***A-B*:** Example experiments of pre- and post-signal coupling with a *narrow* (***A***) or *wide* (***B***) time interval in control and in presence of ifenprodil (10 μM) conditions. ***C***: Summary of experiment data in (***A***) and (***B***). Blue shading corresponds to narrow Δt while pink shading indicates wide Δt. ***D***: Bar graphs represent the statistics in (***C***).

4.2.3 Discussions – Paper II

NMDA-mediated calcium is essential for tLTP formation in the striatum (Shen, Flajolet et al. 2008) (also e.g. in paper I). However, it is not known how subunits of NMDARs shape the tLTP formations at corticostriatal synapses in MSNs. In this study, we investigated tLTP formation with different GluN2 subunits in a biophysically detailed model. The model predicted that during the tLTP induction, GluN2A and GluN2B subunits generate highest calcium elevations (normalized to base level). In particular, GluN2B induced a broad calcium curve as a function of inter-stimulus interval (Δt) in the tLTP protocol, suggesting a wide timing window between pre- and post-synaptic signals for tLTP induction. To demonstrate the role of GluN2B subunit, we performed the STDP experiment in control and in presence of GluN2B blocker. Our experiments confirmed that presence of GluN2B allow a broader timing-window for tLTP, while inhibiting GluN2B and leaving GluN2A alone would prevent tLTP formation with a wide Δt. Thus, the balance of GluN2A and GluN2B would shape the STDP curves. GluN2A would narrow the STDP curve and fine tune cortical inputs, while GluN2B might play roles in a broader integration of cortical inputs. These findings might allow us to better understanding functional importance of GluN2A and GluN2B subunits in neural disorders such as Parkinson's (Hallett and Standaert 2004) and Huntington's (Li, Fan et al. 2003) disease model.

4.3 DENDRITIC PLATEAUS SHAPE THE SPATIOTEMPORAL INTEGRATION WINDOW FOR BOTH EXCITATORY AND INHIBITORY INPUTS IN STRIATAL MSNS (PAPER III)

A synaptic barrage could lead to strong depolarization, termed as “dendritic plateaus”, in striatal MSNs lasting for hundreds of milliseconds (Plotkin, Day et al. 2011). However, it is not known: (1) how could dendritic plateaus affect the integration of other excitatory signals and turn them into spikes? (2) how could dendritic inhibition shapes this plateau-dependent phenomena?

To answer these questions, we have built a morphologically more realistic, biophysically detailed model of the MSN. The mode was tuned to fit current experimental conditions (Figure 4) and was able to generate dendritic plateaus similar to plateaus we induced experimentally via 2-phto uncaging or local electrical stimulations (Figure 13A,B). Using the model, we found that clustered activation of spines more distally gave rise to long-lasting plateau potentials. In contrast, clustered activation of spines more proximally gave rise to “transient” depolarization (Figure 13C), which is consistent with previous published data (Plotkin, Day et al. 2011) as well as in our own experiments. To conclude, the model could faithfully reproduce plateau potentials as in experimental data.

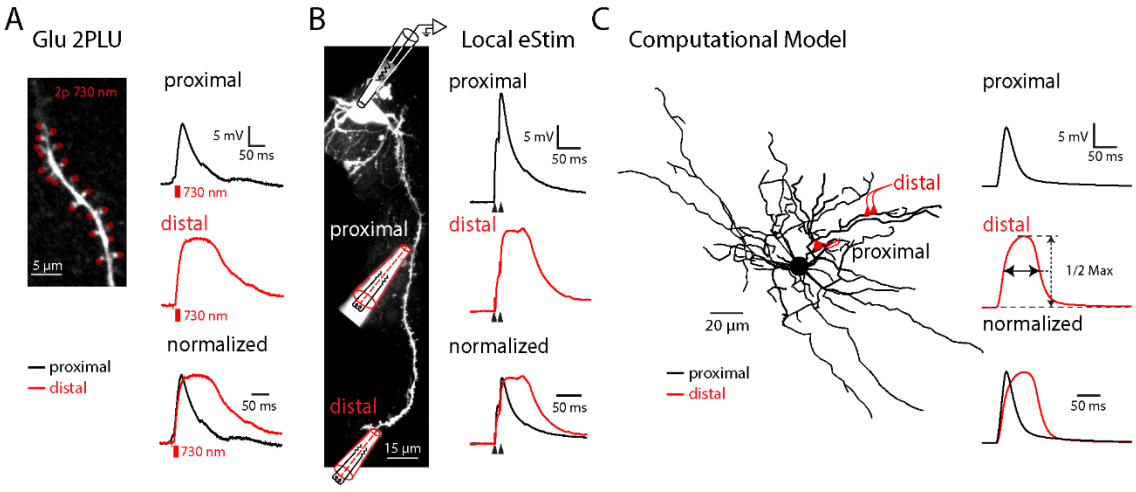

Figure 13 Dendritic plateaus generated in MSN dendrites **(A)** Dendritic plateau induced by 2-photon glutamate uncaging (Glu 2PLU). *Left*, a representative 2-photon image of a MSN dendrite. Red dots indicate the locations for uncaging (730 nm). *Right*, EPSPs induced by glutamate uncaging at 20 spines at proximal or distal dendrites (0.8 ms pulses, ISI = 1 ms). **(B)** Dendritic plateau evoked by local electrical stimulation (eStim) in the presence of PTX (50 µM). *Left,* stimulation locations. *Right*, EPSPs induced by local eStim (2 pulses with 10 ms interval) in the proximal or distal dendrite. **(C)** Dendritic plateaus generated in a detailed MSN model with 634 compartments (left). 15 spines were activated (ISI = 1 ms) at either “proximal” or “distal” dendrites. *Right*, Example somatic voltage traces generated by simulation.

4.3.1 Dendritic plateaus enables neuron-wide integration of excitatory inputs

To investigate how dendritic plateaus and "transient" depolarization could integrate excitatory inputs, we coupled clustered inputs at distal or proximal dendrites with random excitatory inputs (Figure 14A,B). 20 excitatory synapses were randomly distributed in the model to mimic ongoing cortical activities (Matyas, Sreenivasan et al. 2010), which fire at 10 Hz and was delayed (Δt_{ext}) to plateau initiation (Figure 14B). The model was also loaded with spontaneous synaptic noise (Figure 14A). To avoid potential bias due to spatial locations of excitatory inputs, we generated a large pool of 1,000 "unbiased" spatial patterns (Method 3.3.5) for the 20 synapses. Our simulations indicated that distal clustered inputs were able to integrate delayed and dispersed excitatory signals and turn them into spikes with high probability (e.g. ~40% even Δt_{ext} =40ms, Figure 14C). In contrast, proximally clustered inputs almost failed to integrate delayed excitatory signals (<5% at Δt_{ext} =40ms, Figure 14C). We next investigated the relationship between firing probability and average distance (to the soma) of 20 excitatory synapses. We found that when coupled to plateau potentials, the excitatory inputs distributed far away in the dendrites could generated similar firing statistics as those near to the soma (Figure 14D). To conclude, these data suggest that a dendritic plateau could broaden the spatiotemporal integration of excitatory inputs to MSNs.

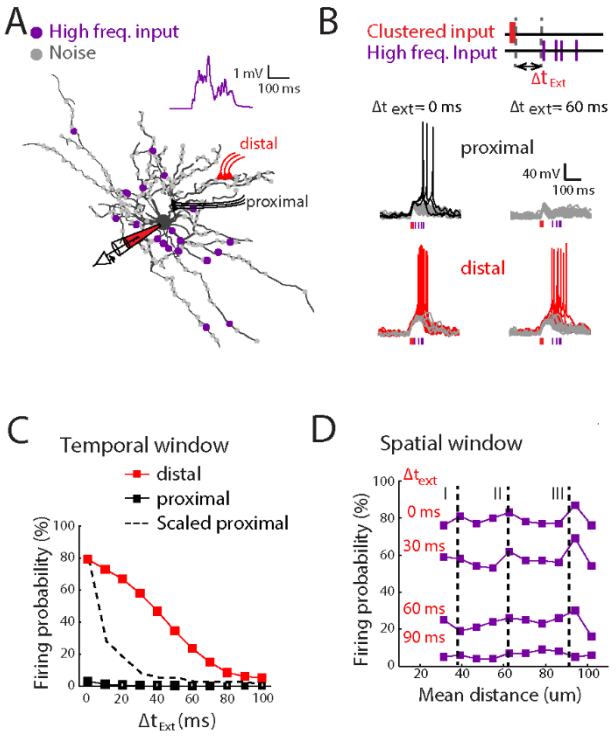

Figure 14 Dendritic plateau potential broadened spatiotemporal integration windows for excitatory inputs. (***A***) The MSN model was loaded with background Poisson noise (grey dots, see Methods). Clustered inputs were activated either distally (red) or proximally (black) in the dendrites. 20 excitatory synapses were randomly distributed in the dendrites (purple dots). Inset: example trace of somatic membrane potential with high frequency input. (***B***) Pairing clustered and high frequency inputs

triggered action potentials. *Upper*, simulated inputs protocol: clustered inputs (red lines; proximal or distal) were followed by high frequency inputs (purple lines) with varied time delay (Δt_{ext}). *Lower*, sample traces of modeled somatic membrane potential fluctuations with Δt_{ext} = 0 ms and 60 ms, respectively. (***C***) The firing probability resulting from high frequency inputs as a function of the time delay between inputs and plateau potential (Δt_{ext}) (n=1,000). The clustered spines were activated either distally (red) or proximally (black) as indicated in (A). The dashed line indicates the scaled firing probability by proximally evoked plateau. (***D***) The firing probability of dendritic plateaus coupled with high frequency inputs at different Δt_{ext} was plotted as a function of mean distance from soma. Dashed lines indicate the mean distance-to-soma of inputs at proximal (I), middle (II) and distal (III) dendrite.

4.3.2 Model predicted a spatiotemporal window for efficient inhibition

How would inhibitory inputs modulate this neuro-wide integration of excitatory inputs? Classic theory highlighted the importance of spatial location for dendritic inhibitions (Mel and Schiller 2004) . It was suggested that the most efficient way for inhibition is to place the GABAergic synapses in the following way: (1) in the distal dendrite where clustered inputs were activated (location 'a', 'on-spot') (Liu 2004), (2) proximally in the activated dendrite (location 'b', 'on-path') (Koch, Poggio et al. 1983), (3) in the perisomatic region (soma) (Galarreta and Hestrin 1998), and (4) dispersed in the neighboring dendrite (location 'c', 'off-path') (Gidon and Segev 2012). Accordingly, we placed 1 (or 2) $GABA_A$ synapses (g_{max}=1,500 pS, E_{GABA} = -60 mV) at the suggested locations . To further identify if the timing of inhibition is important, we varied the delay (Δt_{Inh}) between the onset of the plateau and the inhibitory input. Surprisingly, we found that if GABA synapses were placed near the plateau initiation zone (location'a' in Figure 15A-B), there is a particular temporal window where the inhibition is most efficient. However, this temporal window seems to disappear if GABAergic inputs were located far away from the plateau initiation zone (Figure 15A-B). To identify if the spatiotemporal window for inhibition was due to the driving force of GABA, we next simulated dynamic current injection, mimicking unitary GABAergic IPSCs (Figure 15C). We repeated the same simulations as in the previous scenario, but with the $GABA_AR$ conductance replaced by dynamic current injections. We found 'on-spot' current injection (location 'a') had strongest impact on firing probability and exhibited a similar temporal profile as seen in simulations using $GABA_AR$ conductance (Figure 15D), suggesting that differences in efficacy of inhibition was not caused by differences in driving forces for Cl^- at different dendritic and somatic locations.

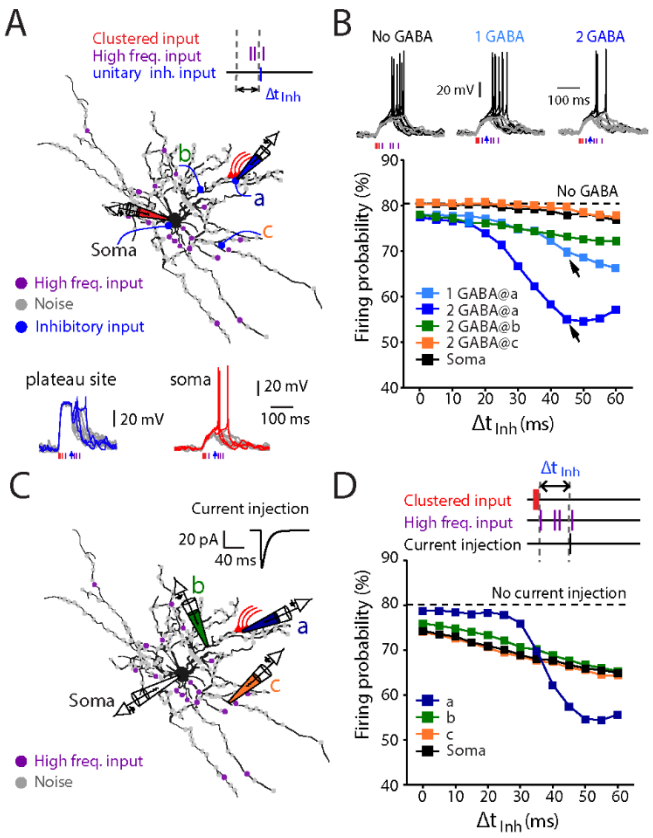

Figure 15: Spatiotemporal window of dendritic inhibition **(A)** The simulation scheme for timing of clustered, high frequency, and inhibitory inputs. In addition to background noise and high frequency inputs, the model MSN was loaded with additional unitary inhibitory inputs. Inhibitory synapses (1 or 2 GABAergic synapses, g_{max}GABA = 1,500 pS, E_{GABA}= -60mV) were placed at selected locations: a (plateau site), b (on the same dendrite proximal to plateau site), c (off branch), and the soma. For each location, inhibitory synapses were activated following the induction of the plateau with a time delay (Δt_{Inh}). *Lower inserts:* example voltage traces (n = 20) were recorded at the "plateau site" (blue curves) or soma (red curves) when 2 GABAergic synapses were activated. Grey traces indicate that no action potential was triggered. **(B)** *Upper:* example simulated somatic voltage traces (20 trials, arrows indicate $GABA_AR$ activation). *Lower*: Firing probabilities (n = 1,000 trials per condition) were plotted as functions of the number and location of GABAergic inputs and the timing (Δt_{Inh}) between clustered inputs and unitary inhibitory input. $GABA_AR$ activation near or on the same branch where dendritic plateau was generated could efficiently decrease the firing probability (2 GABA@a, 1 GABA@a). **(C)** The simulation procedure was the same as in (A), but GABAergic synapses were replaced with transient IPSC-like current injections (inset) at selected locations (a - c, soma). **(D)** Firing probabilities were plotted as a function of current injection timing.

4.3.3 Possible effects of different intrastriatal inhibitory interneurons

A unique feature of the striatum is that it is nearly purely GABAergic and completely lack intrinsically excitatory neurons (Tepper, Koos et al. 2004, Gittis and Kreitzer 2012) . In order to investigate different sources of intrastriatal inhibition, we simulated three major types of inhibition: (1) typical FSI-mediated perisomatic inhibition with fast kinetics (FS GABA); (2) dendritic inhibition with fast kinetics (fGABA) resembling lateral inhibition between MSNs; (3) neuropeptide Y–expressing neurogilaform (NPY-NGF) interneuron-mediated dendritic

inhibition with slow kinetics (sGABA) (details for all these types of $GABA_AR$s can be found in table 4, Method 3.3.3) (Galarreta and Hestrin 1998, Taverna, Ilijic et al. 2008, Ibanez-Sandoval, Tecuapetla et al. 2011). When modeling FSI input trains (firing at 30Hz for 200 ms) to MSNs, we put 10 (or 20) FSI $GABA_AR$ with short-term depression plasticity (Planert, Szydlowski et al. 2010) on the soma (Figure 16A). In comparison, we placed two fGABA (or sGABA) close to the plateau initiation site (Figure 16A). Our simulation results showed that somatic inhibitions such as FSI input trains had relatively weak effects on suppressing the plateau coupled excitation (Figure 16B). In contrast, activating unitary fGABA conductance in the temporal window (30-40ms delayed following the plateau initiation) could more effectively the plateau induced spiking (Figure 16B). Noticeably, activation of two unitary $sGABA_AR$ strongly inhibited the plateau-dependent spiking (Figure 16B). Taken together, the optimal spatiotemporal window for inhibition allows dendritic inhibition to control the plateau-coupled excitation more effectively than somatic inhibition in the MSNs displaying plateaus.

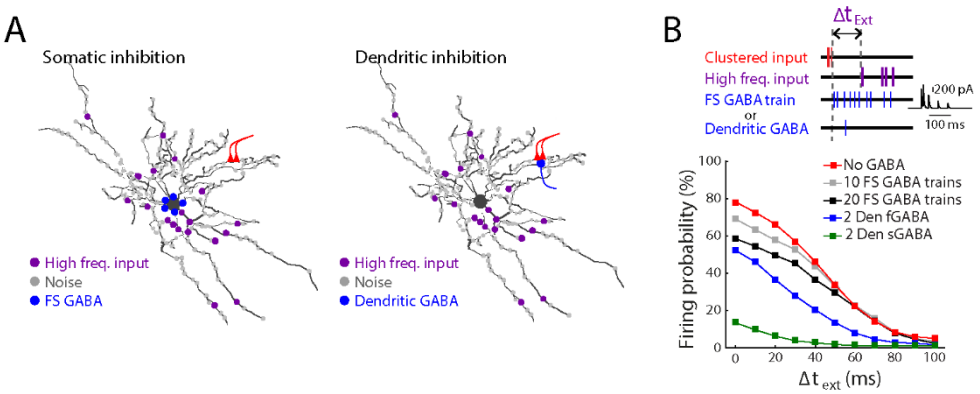

Figure 16. Dendritic VS somatic inhibtion in the striatum. **(A)** Distribution of synaptic inputs used for simulation (*left*, perisomatic inhibition; *right*, dendritic inhibition). **(B)** The effect of different types of inhibition patterns on temporal integration of excitation. Firing probability is plotted as function of excitation timing (Δt_{Ext}), with fixed timing for FS or dendritic inhibition. Dendritic inhibition provided broadened temporal tuning capacity compared to perisomatic high frequency inhibitory trains.

4.3.4 Mg^{2+}-dependent mechanism important for effective inhibitory control of dendritic plateaus

What could be the mechanism that accounts for the spatiotemporal window of dendritic fGABA? The efficacy of the inhibitory synaptic input could be jointly determined by driving force of the synaptic channels and local input resistance. Our previous results indicated the spatiotemporal window for dendritic fGABA was not due to driving force of Cl^- (Figure 15B). Thus we focused on the possible impact of dendritic input resistance. In order to capture the fine details of dendritic responsiveness, we examined the transient-state of the dendritic membrane potential perturbations in response to short pulses in our MSN model

(Figure 17A). To distinguish responsiveness to excitatory and inhibitory inputs at local dendritic compartments, we injected either depolarized or hyperpolarized current test pulses (4- 20 ms duration, 20 pA, meant to mimic IPSCs). By shifting the timing of the current injection with a small step (2 ms), we obtained consecutive transient states in the dendritic responsiveness, measured by subtracted local membrane potential perturbation (ΔV) (Figure 17B). Strikingly, we found that the ratio between the amplitude of the excitatory and the inhibitory perturbations (E/I) followed a *bi-phasic* distribution (Figure 17C), while the "inhibition phase" (E/I < 1) arose before the "excitation phase" (E/I > 1). Such a temporal window is consistent with our previous simulation examining the effect of dendritic inhibition on spiking probability (Figure 15A). Interestingly, with the location gradually shifting away from the plateau initiation zone to the soma, the bi-phasic ratio appears to vanish, suggesting a spatial window for favoring inhibition. Taken together, the bi-phasic ratio measured by the short pulses suggests a spatial and temporal window that could amplify the efficiency of inhibition, consistent with our previous observation of a spatiotemporal window for dendritic fGABA channels.

What is the mechanism underlying the bi-phasic |ΔV| responsiveness in the local dendrite after a dendritic plateau is generated? Calcium channels are known to increase the duration of dendritic plateaus on MSNs (Plotkin, Day et al. 2011). We first assessed contributions of ion channels. However, even if we removed all ion channels in the plateau initiation branch, the bi-phasic |ΔV| responsiveness still existed (data not shown), suggesting ion channels might influence on the shape of the plateau, but not affect the bi-phasic |ΔV| responsiveness. In addition to voltage-gated ion channels, NMDAR-mediated currents are critical for plateau generation and dendritic non-linearity (Schiller, Major et al. 2000). We next focused on the role of NMDARs. To rule out contributions by ion channels, the plateau induction was repeated in a pure passive MSN model (Figure 17C). Interestingly, we found the bi-phasic distribution of |ΔV| responsiveness was very sensitive to extracellular magnesium concentration ($[Mg]^{2+}$). By varying $[Mg]^{2+}$ in our model, color-coded bi-phasic E/I response curves faded with lowered $[Mg^{2+}]$ (Figure 17D). In Mg^{2+} free condition, the bi-phasic ratio completely vanished (Figure 17D)! These simulation results suggest that the Mg^{2+} block of NMDARs is the determining factor for dendritic inhibition after the dendritic plateau is induced.

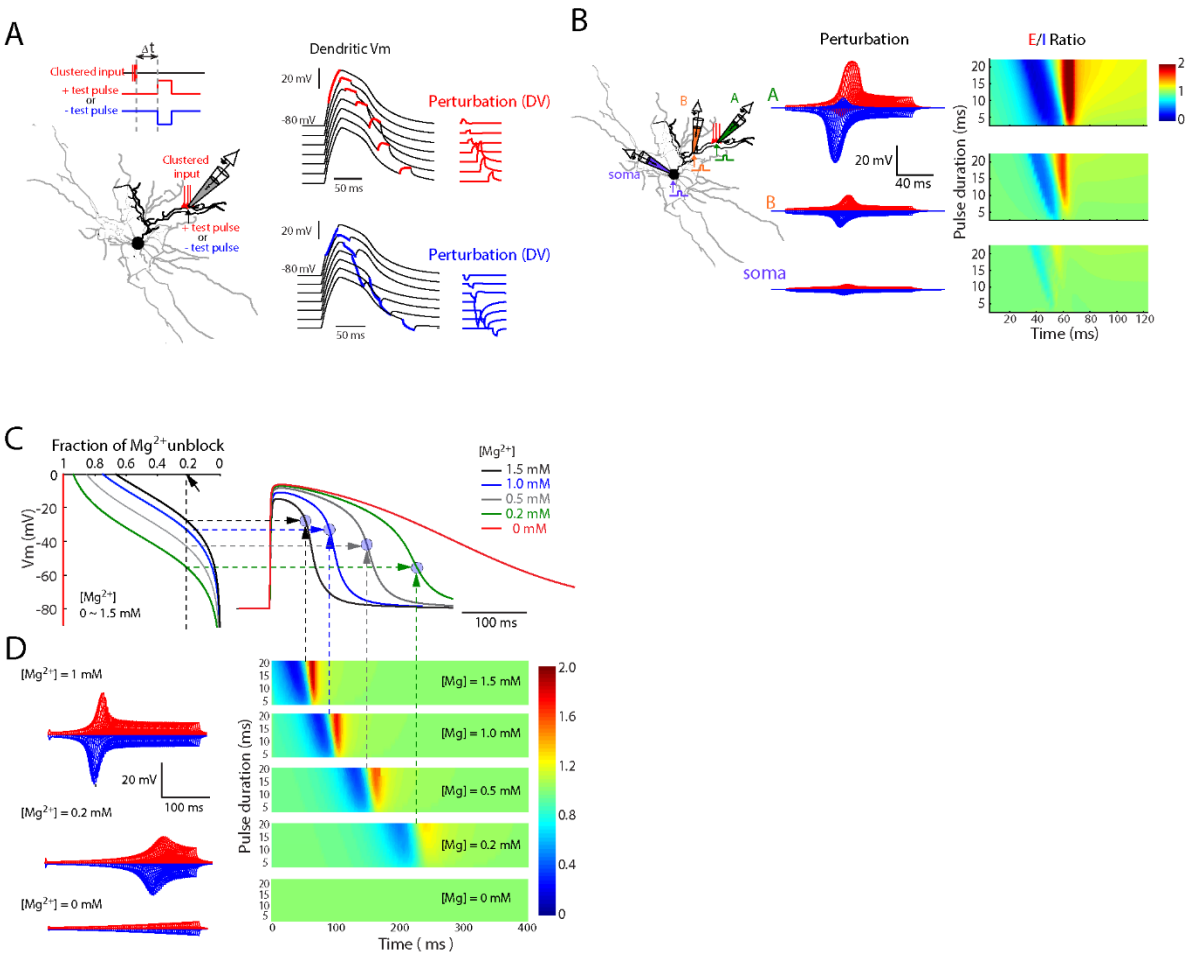

Figure 17. **(A)** Schematic for simulation of membrane potential perturbation (|ΔV|) in response to a short current injection (test pulse). *Left*, dendritic plateau was induced by activation of distal clustered inputs. Current injection and local membrane potential measurements were achieved by a simulated local patch clamp electrode. *Middle*, example traces of local dendritic membrane potential fluctuation in response to test pulse current injections: +20 pA (*red*) or –20 pA (*blue*) for 20 ms with varied timing (Δt). *Right*, subtracted traces of membrane potential perturbation. **(B)** Spatial profiles of the E/I ratio at selected locations (a: plateau site, b: proximal to the plateau site, and Soma). Note that the bi-phasic E/I ratio was most prominent in the distal dendrite where the plateau was generated. **(C-D)** Exploring mechanism underlying the biphasic "E/I" in a pure passive MSN model. **(C)** Effects of extracellular Mg^{2+} concentration ($[Mg^{2+}]$) on dendritic plateaus. *Left*, fraction of Mg^{2+}-unblock. *Right*, sample traces of the plateau induced by 15 synapses with different $[Mg^{2+}]$. **(D)** Effects of $[Mg^{2+}]$ on the E/I ratio. *Left*, sample traces of excitatory and inhibitory |ΔV| with different $[Mg^{2+}]$. *Right*, heat-maps show E/I ratios under different $[Mg^{2+}]$. Note that the strength of the bi-phasic E/I ratio faded when $[Mg^{2+}]$ approached 0 mM. In Mg^{2+}-free situation, the bi-phasic phenomenon vanished. The balance points (defined by E/I ratio = 1) could be predicted by ~20% Mg^{2+}-unblock in different $[Mg^{2+}]$ conditions.

4.3.5 Verification of Mg^{2+}-dependent mechanism with uncaging of glutamate and GABA

Our simulations predicted a branch-specific inhibition on the plateau-coupled excitation. In addition, the branch-specific inhibition is dependent on the Mg^{2+} block of NMDARs. Therefore we aimed to verify our predictions with experiments. To precisely control the

timing and locations for excitatory and inhibitory input patterns, our collaborators adopted dual color 1-photon GABA (20µM Rubi-GABA in blue lights of 450 nm) and 2-photon glutamate (0.7 mM DNI-Glu in red lights of 730 nM) uncaging (Figure 18A). Compared to another compound MNI-Glu, DNI-Glu only mildly inhibits $GABA_A$Rs (Chiovini, Turi et al. 2014) and allow the induction of IPSCs via GABA uncaging in the presence of DNI-Glu. 2PLU uncaging of DNI-Glu at clustered spines (pulse width = 0.8 ms, ISI = 1 ms, 20 spines) along the distal dendrite could generate a dendritic plateau (Figure 18B). Uncaging GABA at the location near plateau initiation branch ('on branch') strongly inhibited the plateau (Figure 18B); by contrast, inducing IPSCs at neighboring branch ('off branch') only mildly attenuate the plateau (Figure 18B): on branch: 40 ± 3%, n = 10 dendrites/ 6 cells, off branch: 11 ± 3%, n = 7 dendrites/ 6 cells, Mann-Whitney, P = 0.0008. Next, the same experiments were performed in Mg^{2+} free condition. Due to removal of Mg^{2+} ions, a plateau potential could be evoked with much longer duration (ACSF: 93 ± 7 ms, n = 10; Mg^{2+}-free: 257 ± 50 ms, n = 12; Mann-Whitney, P = 0.0003, Figure 18C) but requiring fewer spines (10 spines). Moreover, the shape of plateaus looked more like NMDA EPSCs (Figure 18C), consistent with the previous model prediction (Figure 17C). However, uncaging GABA 'on branch' appears to have weak inhibition effects similar to uncaging GABA at 'off-branch' (Δduration: on branch: 12 ± 3 %, n = 12 dendrites/ 6 cells; off branch: 6 ± 4 %, n = 10 dendrites/ 6 cells, Mann-Whitney, P = 0.2766, Figure 18C). Taken together, using *ex vivo* uncaging experiment it was demonstrated that the branch-specific inhibition is not due to shunting effects of GABA, but indeed relied on Mg^{2+}-block of NMDARs.

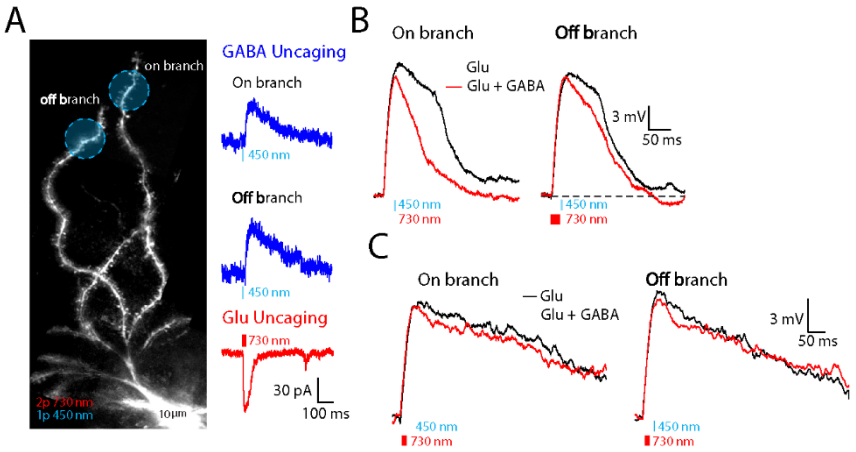

Figure 18. Uncaging glutamate and GABA in control and Mg-free conditions **(A)** *Left*, experimental configuration illustrating locations for 2-photon glutamate uncaging (red dots: 730 nm; DNI-caged glutamate 700 µM) and 1-photon GABA uncaging (blue area: diameter = ~ 19 µm; 450 nm; Rubi-GABA 20 µM). *Right*, uIPSCs (blue) and uEPSC (red) evoked by 1p GABA and 2p glutamate uncaging, respectively. **(B)** *Left*, Representative traces of dendritic plateaus induced by 2-photon glutamate uncaging (black) and subsequent 1-photon GABA uncaging (red) at on branch (left) or off branch (right) locations. *Right*, the effect of GABA uncaging on the duration of dendritic plateau (on branch: n = 10 dendrites/6 cells, off branch: n = 7 dendrites/6 cells, Mann-Whitney, p = 0.0008). **(C)** *Left*, representative traces of dendritic plateau potentials induced by 2-photon glutamate uncaging with (black) and without (red) on or off branch 1-photon GABA uncaging in Mg^{2+}-free ACSF. *Right*,

the change of dendritic plateau duration induced by on branch GABA uncaging was not significantly different from that of off branch GABA uncaging in Mg^{2+}-free ACSF (on branch: n = 12 dendrites/6 cells, off branch: n = 10 dendrites/6 cells, Mann-Whitney, p = 0.2766).

4.3.6 Discussions – Paper III

Dendritic plateaus are long-lasting depolarizations generated by spatiotemporally clustered excitatory inputs at distal dendrites. In this study, we investigated: (1) how dendritic plateaus can help integrate later incoming excitatory signals and (2) how this plateau-coupled excitation is modulated by dendritic inhibition in MSNs. The simulations predicted that the plateau potential greatly strengthen MSN's capacitance of integrating temporally delayed and spatially "neuron-wide" excitatory signals. In contrast, model predicted a narrow spatiotemporal window for dendritic fast inhibition; that is, to maximize its efficacy, inhibition has to be close to the plateau initiation zone and activated within a particular timing-window. The model predicted a *bi-phasic* balance between excitatory and inhibitory responsiveness curves, which could account for the spatiotemporal effects of inhibition. Further, the bi-phasic ratio of dendritic responsiveness curves relies on Mg^{2+} block of NMDARs. We demonstrated the Mg^{2+} block dependent branch-specific inhibition with uncaging glutamate and GABA experiments.

One important concept we introduced in this study is the 'transient' dendritic responsiveness, instead of focusing on conventional 'steady-state' of the responsiveness. Our consideration is that most of the synaptic events, such as $GABA_A$A and AMPA, with fast kinetics, might cause *transient* perturbation in membrane potentials. Using a steady-state input would fail to capture fine details in dendritic responsiveness to fast synaptic events (Rall and Rinzel 1973, Rinzel and Rall 1974) . Our model predictions and experiments confirmed that transient perturbations were due to Mg^{2+} block of NMDARs, a mechanism that could not simply be interpreted with "classic" cable theory and GABA shunting effects.

Dendritic plateaus are important for the integration of excitatory inputs in the striatum. First, plateaus may be efficient for driving MSNs from a 'down-state' to an 'up-state', because only a few synapse were needed (Plotkin, Day et al. 2011) compared to the case that hundreds of synapse are required if they fire randomly in a non-clustered manner (Wilson and Kawaguchi 1996, Stern, Kincaid et al. 1997, Stern, Jaeger et al. 1998, Wolf, Moyer et al. 2005) . Secondly, plateaus increased the temporal window for MSNs to 'read' cortical information. At last, the plateau potential also strengthens spatial integration of cortical information in dendrites.

As said, the striatum is internally inhibitory circuitry. MSNs are e.g. innervated by inhibitory inputs from three major inhibitory sources: PV-positive FSIs, SST-/NPY-positive LTS interneurons, and neighboring MSNs (Gittis and Kreitzer 2012). Although connectivity and synaptic strength of different striatal inhibitions have been extensively studied, their functional impact remain unclear. In this study, our results suggested that the neuro-wide

excitation evoked by plateau potentials could be controlled by only a few GABA synapses if they are close to the plateau initiation zone and activated with a particular timing. Activation of several GABAA synapses in the spatiotemporal window are much more powerful than perisomatic inhibition from FSIs. In addition, slow-$GABA_A$ such as the inputs from NPY-NGF neurons are potent in suppressing the plateaus. Despite NPY-NGF interneurons are very few in numbers, considering the high connectivity (%60-87%) between MSNs and NPY-NGF neurons (Ibanez-Sandoval, Tecuapetla et al. 2011, Luo, Janssen et al. 2013), NPY-NGF interneurons might still play a significant role in the striatum to control dendritic plateaus and their associated neuron-wide integration of excitatory inputs.

5 CONCLUSIONS AND FUTURE PERSPECTIVES

In this thesis, we have explored non-linear signal integration in dendrites using biophysically detailed neuron models in close interactions with experimentalists who also helped to verify several model predictions.

In paper I, we investigated how GABAergic inputs could affect the polarity of STDP at corticostriatal synapses in MSNs. Our results indicated GABAergic inputs depolarized the dendrites and the depolarization effects altered the balance of NMDA-mediated calcium and L-type calcium. The depolarization effects of GABA could be attributed to differences between the local dendritic membrane potential and the $GABA_AR$ driving force (measured at approximate -60 mV via cell-attached recordings) during the STDP protocols. One critical question which is not fully addressed in Paper I is that where the GABAergic inputs come from. The model predicted that GABA could potently depolarize the distal dendrites but due to highly leaky dendrites (dense Kir channels), the depolarization effects could not be observed in the soma. The model also suggested that in order to create such depolarization, there should be sufficient amount of GABA inputs at local dendrites. What could these GABA inputs come from? One plausible explanation is from FSIs. During our experimental STDP protocols, in order to obtain 'stable' EPSCs ranging from 50-200 pA in recorded MSNs, we strongly activated cortex via electrode stimulations. The cortical stimulation didn't simply evoke EPSCs in MSNs, but always triggered 1-2 spikes in FSIs that were measured (data not shown). Considering one MSN could be contacted by 5-20 FSIs (Wilson 2007), it could receive plenty of GABAerigc inputs from FSIs. However, what is puzzling is that FSIs may mainly target perisomatic regions of MSNs (Tepper, Koos et al. 2004) . Recently, however, using optogenetic activation of FSI terminals along MSN dendrites, FSIs were found to also target more distal parts of MSN dendrites up to 100µm from the soma (Straub, Saulnier et al. 2016). More circuitry-breaking experiments are required to identify the timing and location of GABAergic inputs during the STDP protocols. Another interesting topic is how the tonic GABA modulate the STDP in MSNs. MSNs are fully covered by extra-synaptic $GABA_ARs$ which are the main sources to generate tonic GABA activities (Ade, Janssen et al. 2008). Tonic GABA differentially modulate D1- and D2-MSNs, in particular potently depolarizing the D2-MSN at rest (Ade, Janssen et al. 2008). Tonic GABA is therefore expected to impact on the polarity of STDP rules in MSNs through depolarizing effects.

In paper II, we investigated the same STDP protocol as in paper I (but with GABA blocked), but here focused on the roles of NMDAR subunits in LTP formation. GluN2A and GluN2B are abundant in the striatum (Chapman, Keefe et al. 2003) and important for motor disorders such as Parkinson's (Hallett and Standaert 2004) and Huntington's disease (Li, Fan et al. 2003). The GluN2 subunits differ in their decay kinetics and Mg^{2+} block parameters, which are critical for dendritic plateau induction and branch-specific inhibition that were shown in paper III. It would be very interesting to further examine how dendritic inhibition would

modulate NMDA spikes/plateaus induced with different GluN2 subunits in control and disease model.

In paper III, we investigated the functional importance of the dendritic plateau, a supralinear excitation form in MSNs. We have shown that plateau potentials could evoke neuron-wide integration of excitatory inputs but could be selectively inhibited by a few GABA synapses if they are activated in a proper spatiotemporal window. One interesting finding in this paper is that we demonstrated Mg^{2+} - block based mechanism for the branch-specific inhibition, which is distinct from classic GABA shunting mechanism. In many classic theoretical studies, exploration of GABA efficacy were based on GABA 'shunting'—leaky ions through GABA channels (Rinzel and Rall 1974, Koch, Poggio et al. 1983, Gidon and Segev 2012). It is worthy to note that AMPA channels were the only 'excitation' form in those studies. Those classic conclusions could perhaps be revisited by taking into account the presence of NMDARs and Mg^{2+} - block based mechanism that we proposed. In the experiment demonstration part, we only verified the spatial location for the branch-specific inhibition, but didn't check the temporal window due to limitation of experimental techniques – activation of $GABA_A$Rs with uncaging GABA could only produce slow IPSCs. The previous simulations predicted that a temporal window could only be seen when fast IPSCs were presented. To obtain more realistic (fast) IPSCs, we will have to optogenetically evoke individual GABAergic terminal of particular interneuron or MSN as in (Straub, Saulnier et al. 2016). This is an ongoing project now performed in our collaborators lab at Stanford. Our preliminary results are quite consistent with model predictions!

Taken all these together, we have shown that dendrites could powerfully influence plasticity formation and excitation-inhibition interactions in MSNs. One intriguing thought is that if the theory of non-linear dendritic integration would be introduced into artificial neural works such as deep learning? It has been proposed that single pyramidal neuron could even compute as a '3-layer ' neural network (Hausser and Mel 2003), which is in sharp contrast to the idea of 'point' neuron in most popular artificial intelligence techniques, such as the convolution neural network in "deep learning" (Hinton, Osindero et al. 2006). The major challenges in merging neuroscience and deep learning lie in many aspects (Marblestone, Wayne et al. 2016). For example, the artificial neural works are critically dependent on a mechanism called "error back-propagation" which can be used to train the weights of the entire network (Psaltis, Sideris et al. 1988, Aleksander and Morton 1990). This mechanism, however, could not work well in spiking neural networks. Moreover, it is not clear how to design "cost function" in a more biological plausible neural network. Interestingly, a recent spiking neural network model provides important hints on how to apply "error back-propagation" in the spiking neural network (Gutig 2016) and perhaps networks with detailed neurons. Another interesting idea is how to design Artificial General Intelligence (AGI) (Goertzel and Pennachin 2007). Although the current deep learning models are powerful in performing particular task, they appear to lack the capacitance of doing general learning, e.g. to learn visual information and auditory information at the same time. MSNs receive inputs from nearly all over cortex, thalamus and hippocampus (Tepper, Koos et al. 2004), which

carry abundant multi-modal information (Reig and Silberberg 2014). Will MSNs and the striatum be a good model system for AGI? To conclude, to integrate up-to-date knowledge of neuroscience and artificial intelligence is one of the most exciting challenges in the next decade!

6 ACKNOWLEDGEMENTS

Time passes so quickly. When I start to write this chapter, I suddenly realized that I have been in Scandinavia for nearly 12 years. During these 12 years, I did my master study, got married, worked as a research student, and am now approaching to complete my PhD degree. Science is essentially a path seeking for the truth, while pursuing truth is a lifelong journey and it is always lonely. I would express my deep and sincere thanks to many friends and my family. Because of you, I never feel alone.

I would like first thank my main supervisor, **Jeanette Hellgren Kotaleski**, who gave me this wonderful opportunity and leads me into the door of science. During the past eight years, you give me great freedom and patience to explore science. From the first day that I entered your lab, whenever I have any question, I just went directly into your office and asked if you 'have 5 minutes' now. You always smiled and said 'yes, I have'. The "5 minutes talk" always extends to one hour and even longer. I now feel so lucky and even luxury that you could spend so much time with me. Among many things you told me, one thing that impressed me most is to fully understand why models would fail, because '*failure is the most common thing that scientists encounter everyday, and learning from mistakes is the most efficient way to success*'. I benefit a lot from these words.

Sten Grillner, my co-supervisor, I would like to thank you for your insightful suggestions and your support for my projects. When I was stuck in science or meet some problems in my life, I can always ask for your advice. I also like a lot the salmon party hosted in your home.

I also thank **Gilad Silberberg**, my co-supervisor. I have spent countless time in discussing with you about the projects and your knowledge has greatly deepen my understanding in the striatal physiology.

I thank many members in our lab. **Robert Lindroos**, who share the office with me during last 3,4 years. I really enjoy my time with you, and we have so many topics every day, from Champion's League to the striatum ☺. **Alexander Kozlov**, thanks for your help in Programming. **Anu**, thanks for your suggestions to my project and to my thesis writing. I also thanks for other members, **Jovana, Johannes, Jan, Olivia and Daniel**, who always give me valuable inputs and stimulus to my ongoing projects.

I thank **Arvind Kumar**. Your opinions are always so sharp and straightforward, but I really enjoy our discussions. This is what science should be.

I thank **Abdel El Manira**. Your course "ion channels and receptors" is one of the best courses I had here at Karolinska, which gave a broad and in-depth overview about those fundamentals in neuroscience. My own research was inspired from the lecture you gave in that course, where you introduced how to measure the input resistance of the cell when synaptic channels open.

I thank **Sten, Abdel, Fisone, Peter, Brita** and **Ole**, who have created this wonderful scientific environment in our department. I thank **Ole** for allowing me to share his magic coffee.

I thank other PhD students in this corridor, **Shreyas, Elham** and **Hsu Li-ju** for numerous pleasant time we spent together.

I am deeply grateful for many collaborators in my papers who I can always learn from. It is my privilege that I can work with so many leading scientists in the field.

I thank for **Ding Jun** at Stanford University and his lab members who warmly hosted my visit to his lab. Your participation in the project has significantly elevated the level of my work! During my half year's stay at Stanford, I really enjoy the scientific atmosphere in your lab. In particular, **Wu Yu-wei**, who is such a skillful and humble scientist. It is always my great pleasure to work with you. I thank **Rupa** for helping with my manuscripts.

I also thank **Laurent Venance, Fino, Avrama Blackwell** and **Evans** who worked with me on many interesting projects.

I thank for my Chinese fellows in Sweden: **Song jianren, Guan Na, Song Huan, Zhu Jianwei, Wang yixin, Yang Dong, Zhang Yuning, Menghan, Song ci, Chang Zheng, Suo Chen, Zhang Qiang, Xuan Yang, Xinming, Celine, Jia Qi, Qiong zi , Gu Tianyu**. 谢谢我的小伙伴们!

A special thanks goes to **Anders Krogh** at University of Copenhagen, who was the supervisor for my master study. Thank you to open the door for me, where I began my journey in science. I also thank **Bjorn**, my co-supervisor for my master thesis at Denmark Technique University (DTU).

I thank my parents, who value science and firmly support me to be a good scientist! 非常感谢父母对我的支持，你们尊重科学的价值观深深的影响到我对科学和博士研究的态度。

I thank for the support from my sister **Du Xin**.

At last, I would like thank my wife, **Qin Xiao**. Without your support, I would never come so far!

7 REFERENCES

Ade, K. K., M. J. Janssen, P. I. Ortinski and S. Vicini (2008). "Differential tonic GABA conductances in striatal medium spiny neurons." Journal of Neuroscience **28**(5): 1185-1197.

Adermark, L. and D. M. Lovinger (2007). "Combined activation of L-type Ca2+ channels and synaptic transmission is sufficient to induce striatal long-term depression." J Neurosci **27**(25): 6781-6787.

Aleksander, I. and H. Morton (1990). An introduction to neural computing, Chapman and Hall London.

Antic, S. D., W. L. Zhou, A. R. Moore, S. M. Short and K. D. Ikonomu (2010). "The Decade of the Dendritic NMDA Spike." Journal of Neuroscience Research **88**(14): 2991-3001.

Ascoli, G. A., D. E. Donohue and M. Halavi (2007). "NeuroMorpho.Org: a central resource for neuronal morphologies." J Neurosci **27**(35): 9247-9251.

Bi, G. Q. and M. M. Poo (1998). "Synaptic modifications in cultured hippocampal neurons: dependence on spike timing, synaptic strength, and postsynaptic cell type." J Neurosci **18**(24): 10464-10472.

Bliss, T. V. and G. L. Collingridge (1993). "A synaptic model of memory: long-term potentiation in the hippocampus." Nature **361**(6407): 31-39.

Bliss, T. V. and A. R. Gardner-Medwin (1973). "Long-lasting potentiation of synaptic transmission in the dentate area of the unanaestetized rabbit following stimulation of the perforant path." J Physiol **232**(2): 357-374.

Bliss, T. V. and T. Lomo (1973). "Long-lasting potentiation of synaptic transmission in the dentate area of the anaesthetized rabbit following stimulation of the perforant path." J Physiol **232**(2): 331-356.

Bower, J. M. and D. Beeman (1998). The Book of GENESIS：Exploring Realistic Neural Models with the GEneral NEural SImulation System, Springer Science & Business Media.

Bower, J. M. and D. Beeman (2007). "Constructing realistic neural simulations with GENESIS." Methods Mol Biol **401**: 103-125.

Branco, T. and M. Hausser (2010). "The single dendritic branch as a fundamental functional unit in the nervous system." Current Opinion in Neurobiology **20**(4): 494-502.

Brunel, N., V. Hakim and M. J. E. Richardson (2014). "Single neuron dynamics and computation." Current Opinion in Neurobiology **25**: 149-155.

Campbell, N. C., C. F. Ekerot, G. Hesslow and O. Oscarsson (1983). "Dendritic Plateau Potentials-Evoked in Purkinje-Cells by Parallel Fiber Volleys in the Cat." Journal of Physiology-London **340**(Jul): 209-223.

Caporale, N. and Y. Dan (2008). "Spike timing-dependent plasticity: a Hebbian learning rule." Annu Rev Neurosci **31**: 25-46.

Carter, A. G. and B. L. Sabatini (2004). "State-dependent calcium signaling in dendritic spines of striatal medium spiny neurons." Neuron **44**(3): 483-493.

Chapman, D. E., K. A. Keefe and K. S. Wilcox (2003). "Evidence for functionally distinct synaptic NMDA receptors in ventromedial versus dorsolateral striatum." Journal of Neurophysiology **89**(1): 69-80.

Chiovini, B., G. F. Turi, G. Katona, A. Kaszas, D. Palfi, P. Maak, G. Szalay, M. F. Szabo, G. Szabo, Z. Szadai, S. Kali and B. Rozsa (2014). "Dendritic spikes induce ripples in parvalbumin interneurons during hippocampal sharp waves." Neuron **82**(4): 908-924.

Cui, G. H., S. B. Jun, X. Jin, M. D. Pham, S. S. Vogel, D. M. Lovinger and R. M. Costa (2013). "Concurrent activation of striatal direct and indirect pathways during action initiation." Nature **494**(7436): 238-242.

Day, M., D. Wokosin, J. L. Plotkin, X. Y. Tian and D. J. Surmeier (2008). "Differential Excitability and Modulation of Striatal Medium Spiny Neuron Dendrites." Journal of Neuroscience **28**(45): 11603-11614.

De Schutter, E. and J. M. Bower (1994). "An active membrane model of the cerebellar Purkinje cell. I. Simulation of current clamps in slice." J Neurophysiol **71**(1): 375-400.

Debanne, D., B. H. Gähwiler and S. M. Thompson (1998). "Long‐term synaptic plasticity between pairs of individual CA3 pyramidal cells in rat hippocampal slice cultures." The Journal of Physiology **507**(1): 237-247.

Ding, J., J. D. Peterson and D. J. Surmeier (2008). "Corticostriatal and thalamostriatal synapses have distinctive properties." Journal of Neuroscience **28**(25): 6483-6492.

Djurfeldt, M., J. Hjorth, J. M. Eppler, N. Dudani, M. Helias, T. C. Potjans, U. S. Bhalla, M. Diesmann, J. H. Kotaleski and O. Ekeberg (2010). "Run-Time Interoperability Between Neuronal Network Simulators Based on the MUSIC Framework." Neuroinformatics **8**(1): 43-60.

English, D. F., O. Ibanez-Sandoval, E. Stark, F. Tecuapetla, G. Buzsaki, K. Deisseroth, J. M. Tepper and T. Koos (2011). "GABAergic circuits mediate the reinforcement-related signals of striatal cholinergic interneurons." Nat Neurosci **15**(1): 123-130.

Fino, E., J. Glowinski and L. Venance (2005). "Bidirectional activity-dependent plasticity at corticostriatal synapses." Journal of Neuroscience **25**(49): 11279-11287.

Froemke, R. C., J. J. Letzkus, B. M. Kampa, G. B. Hang and G. J. Stuart (2010). "Dendritic synapse location and neocortical spike-timing-dependent plasticity." Front Synaptic Neurosci **2**: 29.

Froemke, R. C., M. M. Poo and Y. Dan (2005). "Spike-timing-dependent synaptic plasticity depends on dendritic location." Nature **434**(7030): 221-225.

Galarreta, M. and S. Hestrin (1997). "Properties of GABA(A) receptors underlying inhibitory synaptic currents in neocortical pyramidal neurons." Journal of Neuroscience **17**(19): 7220-7227.

Galarreta, M. and S. Hestrin (1998). "Frequency-dependent synaptic depression and the balance of excitation and inhibition in the neocortex." Nat Neurosci **1**(7): 587-594.

Gambino, F., S. Pages, V. Kehayas, D. Baptista, R. Tatti, A. Carleton and A. Holtmaat (2014). "Sensory-evoked LTP driven by dendritic plateau potentials in vivo." Nature **515**(7525): 116-+.

Gerdeman, G. L., J. Ronesi and D. M. Lovinger (2002). "Postsynaptic endocannabinoid release is critical to long-term depression in the striatum." Nature neuroscience **5**(5): 446-451.

Gerfen, C. R. (1992). "The neostriatal mosaic: multiple levels of compartmental organization in the basal ganglia." Annu Rev Neurosci **15**: 285-320.

Gerfen, C. R. and D. J. Surmeier (2011). "Modulation of Striatal Projection Systems by Dopamine." Annual Review of Neuroscience, Vol 34 **34**: 441-466.

Gertler, T. S., C. S. Chan and D. J. Surmeier (2008). "Dichotomous Anatomical Properties of Adult Striatal Medium Spiny Neurons." Journal of Neuroscience **28**(43): 10814-10824.

Gewaltig, M.-O. and M. Diesmann (2007). "NEST (neural simulation tool)." Scholarpedia **2**(4): 1430.

Gidon, A. and I. Segev (2012). "Principles Governing the Operation of Synaptic Inhibition in Dendrites." Neuron **75**(2): 330-341.

Gittis, A. H. and A. C. Kreitzer (2012). "Striatal microcircuitry and movement disorders." Trends in Neurosciences **35**(9): 557-564.

Gittis, A. H., A. B. Nelson, M. T. Thwin, J. J. Palop and A. C. Kreitzer (2010). "Distinct roles of GABAergic interneurons in the regulation of striatal output pathways." J Neurosci **30**(6): 2223-2234.

Goertzel, B. and C. Pennachin (2007). Artificial general intelligence, Springer.

Gutig, R. (2016). "Spiking neurons can discover predictive features by aggregate-label learning." Science **351**(6277): 1041-+.

Hallett, P. J. and D. G. Standaert (2004). "Rationale for and use of NMDA receptor antagonists in Parkinson's disease." Pharmacology & Therapeutics **102**(2): 155-174.

Hashimotodani, Y., T. Ohno-Shosaku, H. Tsubokawa, H. Ogata, K. Emoto, T. Maejima, K. Araishi, H. S. Shin and M. Kano (2005). "Phospholipase C beta serves as a coincidence detector through its Ca2+ dependency for triggering retrograde endocannabinoid signal." Neuron **45**(2): 257-268.

Hashimotodani, Y., T. Ohno-Shosaku, M. Watanabe and M. Kano (2007). "Roles of phospholipase Cbeta and NMDA receptor in activity-dependent endocannabinoid release." J Physiol **584**(Pt 2): 373-380.

Hausser, M. and B. Mel (2003). "Dendrites: bug or feature?" Curr Opin Neurobiol **13**(3): 372-383.

Hebb (1949). The Organization of Behavior; A Neuropsychological Theory, New York: Wiley. xix.

Hepburn, I., W. Chen, S. Wils and E. De Schutter (2012). "STEPS: efficient simulation of stochastic reaction–diffusion models in realistic morphologies." BMC systems biology **6**(1): 1.

Hines, M. (1984). "Efficient Computation of Branched Nerve Equations." International Journal of Bio-Medical Computing **15**(1): 69-76.

Hines, M. L. and N. T. Carnevale (1997). "The NEURON simulation environment." Neural Comput **9**(6): 1179-1209.

Hines, M. L., T. Morse, M. Migliore, N. T. Carnevale and G. M. Shepherd (2004). "ModelDB: A Database to Support Computational Neuroscience." J Comput Neurosci **17**(1): 7-11.

Hinton, G. E., S. Osindero and Y. W. Teh (2006). "A fast learning algorithm for deep belief nets." Neural Comput **18**(7): 1527-1554.

Hodgkin, A. L. and A. F. Huxley (1952). "Currents carried by sodium and potassium ions through the membrane of the giant axon of Loligo." J Physiol **116**(4): 449-472.

Hodgkin, A. L. and A. F. Huxley (1952). "A quantitative description of membrane current and its application to conduction and excitation in nerve." J Physiol **117**(4): 500-544.

Ibanez-Sandoval, O., F. Tecuapetla, B. Unal, F. Shah, T. Koos and J. M. Tepper (2011). "A Novel Functionally Distinct Subtype of Striatal Neuropeptide Y Interneuron." Journal of Neuroscience **31**(46): 16757-16769.

Iftinca, M., B. E. Mckay, T. P. Snutch, J. E. McRory, R. W. Turner and G. W. Zamponi (2006). "Temperature dependence of T-type calcium channel gating." Neuroscience **142**(4): 1031-1042.

Ito, M. and M. Kano (1982). "Long-lasting depression of parallel fiber-Purkinje cell transmission induced by conjunctive stimulation of parallel fibers and climbing fibers in the cerebellar cortex." Neurosci Lett **33**(3): 253-258.

Jadi, M., A. Polsky, J. Schiller and B. W. Mel (2012). "Location-dependent effects of inhibition on local spiking in pyramidal neuron dendrites." PLoS Comput Biol **8**(6): e1002550.

James M. Bower and D. Beeman (2003). The Book of GENESIS.

Kawaguchi, Y. (1993). "Physiological, morphological, and histochemical characterization of three classes of interneurons in rat neostriatum." J Neurosci **13**(11): 4908-4923.

Kiehn, O., B. R. Johnson and M. Raastad (1996). "Plateau properties in mammalian spinal interneurons during transmitter-induced locomotor activity." Neuroscience **75**(1): 263-273.

Koch, C., T. Poggio and V. Torre (1983). "Nonlinear interactions in a dendritic tree: localization, timing, and role in information processing." Proc Natl Acad Sci U S A **80**(9): 2799-2802.

Kreitzer, A. C. and R. C. Malenka (2005). "Dopamine modulation of state-dependent endocannabinoid release and long-term depression in the striatum." J Neurosci **25**(45): 10537-10545.

Kubota, Y. and Y. Kawaguchi (2000). "Dependence of GABAergic synaptic areas on the interneuron type and target size." J Neurosci **20**(1): 375-386.

Larkum, M. E., T. Nevian, M. Sandler, A. Polsky and J. Schiller (2009). "Synaptic Integration in Tuft Dendrites of Layer 5 Pyramidal Neurons: A New Unifying Principle." Science **325**(5941): 756-760.

Laurie, D. J. and P. H. Seeburg (1994). "Ligand Affinities at Recombinant N-Methyl-D-Aspartate Receptors Depend on Subunit Composition." European Journal of Pharmacology-Molecular Pharmacology Section **268**(3): 335-345.

Lavzin, M., S. Rapoport, A. Polsky, L. Garion and J. Schiller (2012). "Nonlinear dendritic processing determines angular tuning of barrel cortex neurons in vivo." Nature **490**(7420): 397-401.

Li, L. J., M. Fan, C. D. Icton, N. S. Chen, B. R. Leavitt, M. R. Hayden, T. H. Murphy and L. A. Raymond (2003). "Role of NR2B-type NMDA receptors in selective neurodegeneration in Huntington disease." Neurobiology of Aging **24**(8): 1113-1121.

Lindroos, R., J. Pieczkowski, K. Du and J. H. Kotaleski (2015). Evaluating dendritic impact using complex and reduced models of medium spiny neurons. INCF Neuroinformatics Congress, Stockholm.

Liu, G. S. (2004). "Local structural balance and functional interaction of excitatory and inhibitory synapses in hippocampal dendrites." Nature Neuroscience **7**(4): 373-379.

London, M. and M. Hausser (2005). "Dendritic computation." Annual Review of Neuroscience **28**: 503-532.

Losonczy, A. and J. C. Magee (2006). "Integrative properties of radial oblique dendrites in hippocampal CA1 pyramidal neurons." Neuron **50**(2): 291-307.

Lovinger, D. M., E. C. Tyler and A. Merritt (1993). "Short- and long-term synaptic depression in rat neostriatum." J Neurophysiol **70**(5): 1937-1949.

Luo, R., M. J. Janssen, J. G. Partridge and S. Vicini (2013). "Direct and GABA-mediated indirect effects of nicotinic ACh receptor agonists on striatal neurones." J Physiol **591**(1): 203-217.

Magee, J. C. and D. Johnston (1997). "A synaptically controlled, associative signal for Hebbian plasticity in hippocampal neurons." Science **275**(5297): 209-213.

Major, G., M. E. Larkum and J. Schiller (2013). "Active Properties of Neocortical Pyramidal Neuron Dendrites." Annual Review of Neuroscience, Vol 36 **36**: 1-+.

Major, G., M. E. Larkum and J. Schiller (2013). "Active properties of neocortical pyramidal neuron dendrites." Annu Rev Neurosci **36**: 1-24.

Marblestone, A. H., G. Wayne and K. P. Kording (2016). "Toward an integration of deep learning and neuroscience." Frontiers in Computational Neuroscience **10**.

Markram, H., W. Gerstner and P. J. Sjostrom (2012). "Spike-timing-dependent plasticity: a comprehensive overview." Front Synaptic Neurosci **4**: 2.

Markram, H., J. Lubke, M. Frotscher and B. Sakmann (1997). "Regulation of synaptic efficacy by coincidence of postsynaptic APs and EPSPs." Science **275**(5297): 213-215.

Markram, H., E. Muller, S. Ramaswamy, M. W. Reimann, M. Abdellah, C. A. Sanchez, A. Ailamaki, L. Alonso-Nanclares, N. Antille, S. Arsever, G. A. Kahou, T. K. Berger, A. Bilgili, N. Buncic, A. Chalimourda, G. Chindemi, J. D. Courcol, F. Delalondre, V. Delattre, S. Druckmann, R. Dumusc, J. Dynes, S. Eilemann, E. Gal, M. E. Gevaert, J. P. Ghobril, A. Gidon, J. W. Graham, A. Gupta, V. Haenel, E. Hay, T. Heinis, J. B. Hernando, M. Hines, L. Kanari, D. Keller, J. Kenyon, G. Khazen, Y. Kim, J. G. King, Z. Kisvarday, P. Kumbhar, S. Lasserre, J. V. Le Be, B. R. Magalhaes, A. Merchan-Perez, J. Meystre, B. R. Morrice, J. Muller, A. Munoz-Cespedes, S. Muralidhar, K. Muthurasa, D. Nachbaur, T. H. Newton, M. Nolte, A. Ovcharenko, J. Palacios, L. Pastor, R. Perin, R. Ranjan, I. Riachi, J. R. Rodriguez, J. L. Riquelme, C. Rossert, K. Sfyrakis, Y. Shi, J. C. Shillcock, G. Silberberg, R. Silva, F. Tauheed, M. Telefont, M. Toledo-Rodriguez, T. Trankler, W. Van Geit, J. V. Diaz, R. Walker, Y. Wang, S. M. Zaninetta, J. DeFelipe, S. L. Hill, I. Segev and F. Schurmann (2015). "Reconstruction and Simulation of Neocortical Microcircuitry." Cell **163**(2): 456-492.

Matyas, F., V. Sreenivasan, F. Marbach, C. Wacongne, B. Barsy, C. Mateo, R. Aronoff and C. C. H. Petersen (2010). "Motor Control by Sensory Cortex." Science **330**(6008): 1240-1243.

Mel, B. W. and J. Schiller (2004). "On the fight between excitation and inhibition: location is everything." Sci STKE **2004**(250): PE44.

Monyer, H., N. Burnashev, D. J. Laurie, B. Sakmann and P. H. Seeburg (1994). "Developmental and Regional Expression in the Rat-Brain and Functional-Properties of 4 Nmda Receptors." Neuron **12**(3): 529-540.

Nair, A. G., U. S. Bhalla and J. Hellgren Kotaleski (2016). "Role of DARPP-32 and ARPP-21 in the Emergence of Temporal Constraints on Striatal Calcium and Dopamine Integration." PLoS Comput Biol **12**(9): e1005080.

Nair, A. G., O. Gutierrez-Arenas, O. Eriksson, P. Vincent and J. Hellgren Kotaleski (2015). "Sensing Positive versus Negative Reward Signals through Adenylyl Cyclase-Coupled GPCRs in Direct and Indirect Pathway Striatal Medium Spiny Neurons." J Neurosci **35**(41): 14017-14030.

Nash, J. E. and J. M. Brotchie (2002). "Characterisation of striatal NMDA receptors involved in the generation of parkinsonian symptoms: intrastriatal microinjection studies in the 6-OHDA-lesioned rat." Mov Disord **17**(3): 455-466.

Nevian, T. and B. Sakmann (2006). "Spine Ca2+ signaling in spike-timing-dependent plasticity." Journal of Neuroscience **26**(43): 11001-11013.

Oldenburg, I. A. and J. B. Ding (2011). "Cholinergic modulation of synaptic integration and dendritic excitability in the striatum." Curr Opin Neurobiol **21**(3): 425-432.

Olson, P. A., T. Tkatch, S. Hernandez-Lopez, S. Ulrich, E. Ilijic, E. Mugnaini, H. Zhang, I. Bezprozvanny and D. J. Surmeier (2005). "G-protein-coupled receptor modulation of striatal Ca(V)1.3 L-type Ca2+ channels is dependent on a Shank-binding domain." Journal of Neuroscience **25**(5): 1050-1062.

Planert, H., S. N. Szydlowski, J. J. J. Hjorth, S. Grillner and G. Silberberg (2010). "Dynamics of Synaptic Transmission between Fast-Spiking Interneurons and Striatal Projection Neurons of the Direct and Indirect Pathways." Journal of Neuroscience **30**(9): 3499-3507.

Plotkin, J. L., M. Day and D. J. Surmeier (2011). "Synaptically driven state transitions in distal dendrites of striatal spiny neurons." Nature Neuroscience **14**(7): 881-U101.

Poirazi, P., T. Brannon and B. W. Mel (2003). "Pyramidal neuron as two-layer neural network." Neuron **37**(6): 989-999.

Psaltis, D., A. Sideris and A. Yamamura (1988). "A multilayered neural network controller." IEEE control systems magazine **8**(2): 17-21.

Rall, W. and J. Rinzel (1973). "Branch Input Resistance and Steady Attenuation for Input to One Branch of a Dendritic Neuron Model." Biophysical Journal **13**(7): 648-688.

Ray, S. and U. S. Bhalla (2008). "PyMOOSE: Interoperable Scripting in Python for MOOSE." Front Neuroinform **2**: 6.

Reig, R. and G. Silberberg (2014). "Multisensory Integration in the Mouse Striatum." Neuron **83**(5): 1200-1212.

Rhodes, P. (2006). "The properties and implications of NMDA spikes in neocortical pyramidal cells." J Neurosci **26**(25): 6704-6715.

Rinzel, J. and W. Rall (1974). "Transient-Response in a Dendritic Neuron Model for Current Injected at One Branch." Biophysical Journal **14**(10): 759-790.

Roberts, P. D. and T. K. Leen (2010). "Anti-hebbian spike-timing-dependent plasticity and adaptive sensory processing." Front Comput Neurosci **4**: 156.

Santhakumar, V., R. T. Jones and I. Mody (2010). "Developmental regulation and neuroprotective effects of striatal tonic GABAA currents." Neuroscience **167**(3): 644-655.

Schiller, J., G. Major, H. J. Koester and Y. Schiller (2000). "NMDA spikes in basal dendrites of cortical pyramidal neurons." Nature **404**(6775): 285-289.

Schiller, J. and Y. Schiller (2001). "NMDA receptor-mediated dendritic spikes and coincident signal amplification." Current Opinion in Neurobiology **11**(3): 343-348.

Schulz, J. M., P. Redgrave and J. N. Reynolds (2010). "Cortico-striatal spike-timing dependent plasticity after activation of subcortical pathways." Front Synaptic Neurosci **2**: 23.

Shen, W., J. L. Plotkin, V. Francardo, W. K. Ko, Z. Xie, Q. Li, T. Fieblinger, J. Wess, R. R. Neubig, C. W. Lindsley, P. J. Conn, P. Greengard, E. Bezard, M. A. Cenci and D. J. Surmeier (2016). "M4 Muscarinic Receptor Signaling Ameliorates Striatal Plasticity Deficits in Models of L-DOPA-Induced Dyskinesia." Neuron **90**(5): 1139.

Shen, W. X., M. Flajolet, P. Greengard and D. J. Surmeier (2008). "Dichotomous dopaminergic control of striatal synaptic plasticity." Science **321**(5890): 848-851.

Shonesy, B. C., X. Wang, K. L. Rose, T. S. Ramikie, V. S. Cavener, T. Rentz, A. J. Baucum, 2nd, N. Jalan-Sakrikar, K. Mackie, D. G. Winder, S. Patel and R. J. Colbran (2013). "CaMKII regulates diacylglycerol lipase-alpha and striatal endocannabinoid signaling." Nat Neurosci **16**(4): 456-463.

Siegelbaum, S. A. and E. R. Kandel (1991). "Learning-related synaptic plasticity: LTP and LTD." Curr Opin Neurobiol **1**(1): 113-120.

Silver, R. A. (2010). "Neuronal arithmetic." Nature Reviews Neuroscience **11**(7): 474-489.

Sjostrom, P. J. and M. Hausser (2006). "A cooperative switch determines the sign of synaptic plasticity in distal dendrites of neocortical pyramidal neurons." Neuron **51**(2): 227-238.

Sjostrom, P. J., G. G. Turrigiano and S. B. Nelson (2003). "Neocortical LTD via coincident activation of presynaptic NMDA and cannabinoid receptors." Neuron **39**(4): 641-654.

Smith, A. D. and J. P. Bolam (1990). "The neural network of the basal ganglia as revealed by the study of synaptic connections of identified neurones." Trends Neurosci **13**(7): 259-265.

Smith, Y., D. V. Raju, J. F. Pare and M. Sidibe (2004). "The thalamostriatal system: a highly specific network of the basal ganglia circuitry." Trends Neurosci **27**(9): 520-527.

Stern, E. A., D. Jaeger and C. J. Wilson (1998). "Membrane potential synchrony of simultaneously recorded striatal spiny neurons in vivo." Nature **394**(6692): 475-478.

Stern, E. A., A. E. Kincaid and C. J. Wilson (1997). "Spontaneous subthreshold membrane potential fluctuations and action potential variability of rat corticostriatal and striatal neurons in vivo." Journal of Neurophysiology **77**(4): 1697-1715.

Straub, C., J. L. Saulnier, A. Bègue, D. D. Feng, K. W. Huang and B. L. Sabatini (2016). "Principles of Synaptic Organization of GABAergic Interneurons in the Striatum." Neuron **92**(1): 84-92.

Stuart, G. J. and N. Spruston (2015). "Dendritic integration: 60 years of progress." Nat Neurosci **18**(12): 1713-1721.

Surmeier, D. J., J. Plotkin and W. X. Shen (2009). "Dopamine and synaptic plasticity in dorsal striatal circuits controlling action selection." Current Opinion in Neurobiology **19**(6): 621-628.

Takahashi, H. and J. C. Magee (2009). "Pathway Interactions and Synaptic Plasticity in the Dendritic Tuft Regions of CA1 Pyramidal Neurons." Neuron **62**(1): 102-111.

Taverna, S., E. Ilijic and D. J. Surmeier (2008). "Recurrent collateral connections of striatal medium spiny neurons are disrupted in models of Parkinson's disease." Journal of Neuroscience **28**(21): 5504-5512.

Tepper, J. M., T. Koos and C. J. Wilson (2004). "GABAergic microcircuits in the neostriatum." Trends in Neurosciences **27**(11): 662-669.

Vargas-Caballero, M. and H. P. C. Robinson (2003). "A slow fraction of Mg2+ unblock of NMDA receptors limits their contribution to spike generation in cortical pyramidal neurons." Journal of Neurophysiology **89**(5): 2778-2783.

Vicini, S., J. F. Wang, J. H. Li, W. J. Zhu, Y. H. Wang, J. A. H. Luo, B. B. Wolfe and D. R. Grayson (1998). "Functional and pharmacological differences between recombinant N-methyl-D-aspartate receptors." Journal of Neurophysiology **79**(2): 555-566.

Wilson, C. J. (2007). "GABAergic inhibition in the neostriatum." Gaba and the Basal Ganglia: From Molecules to Systems **160**: 91-110.

Wilson, C. J. and Y. Kawaguchi (1996). "The origins of two-state spontaneous membrane potential fluctuations of neostriatal spiny neurons." Journal of Neuroscience **16**(7): 2397-2410.

Witten, I. B., S. C. Lin, M. Brodsky, R. Prakash, I. Diester, P. Anikeeva, V. Gradinaru, C. Ramakrishnan and K. Deisseroth (2010). "Cholinergic interneurons control local circuit activity and cocaine conditioning." Science **330**(6011): 1677-1681.

Wolf, J. A., J. T. Moyer, M. T. Lazarewicz, D. Contreras, M. Benoit-Marand, P. O'Donnell and L. H. Finkel (2005). "NMDA/AMPA ratio impacts state transitions and entrainment to oscillations in a computational model of the nucleus Accumbens medium spiny projection neuron." Journal of Neuroscience **25**(40): 9080-9095.

Wolf, J. A., J. T. Moyer, M. T. Lazarewicz, D. Contreras, M. Benoit-Marand, P. O'Donnell and L. H. Finkel (2005). "NMDA/AMPA ratio impacts state transitions and entrainment to oscillations in a computational model of the nucleus accumbens medium spiny projection neuron." J Neurosci **25**(40): 9080-9095.

Wu, Y. W., J. I. Kim, V. L. Tawfik, R. R. Lalchandani, G. Scherrer and J. B. Ding (2015). "Input- and cell-type-specific endocannabinoid-dependent LTD in the striatum." Cell Rep **10**(1): 75-87.

Xu, N. L., M. T. Harnett, S. R. Williams, D. Huber, D. H. O'Connor, K. Svoboda and J. C. Magee (2012). "Nonlinear dendritic integration of sensory and motor input during an active sensing task." Nature **492**(7428): 247-+.

Yagishita, S., A. Hayashi-Takagi, G. C. Ellis-Davies, H. Urakubo, S. Ishii and H. Kasai (2014). "A critical time window for dopamine actions on the structural plasticity of dendritic spines." Science **345**(6204): 1616-1620.

Yunker, A. M. R., A. H. Sharp, S. Sundarraj, V. Ranganathan, T. D. Copeland and M. W. McEnery (2003). "Immunological characterization of T-type voltage-dependent calcium channel Ca(V)3.1 (alpha1G) and Ca(V)3.3 (alpha1l) isoforms reveal differences in their localization, expression, and neural development." Neuroscience **117**(2): 321-335.

Zador, A., C. Koch and T. H. Brown (1990). "Biophysical Model of a Hebbian Synapse." Proceedings of the National Academy of Sciences of the United States of America **87**(17): 6718-6722.